Journal of Green Energy Research and Innovation

A New Method for DFIG Control under Unbalanced Grid Voltage Conditions

Mohammad Naser Hashemnia, Ali Dehghan Nayeri

Highlight

- Conducting a thorough examination of DFIG performance in the presence of unbalanced grid voltage conditions
- Presenting two strategies aimed at mitigating active and reactive power oscillations
- Introducing a high selectivity filter (HSF) to separate the fundamental component of stator phase currents from the harmonic components
- Demonstrating the effectiveness of the proposed method compared to traditional DPC controllers through extensive simulations

Graphical Abstract

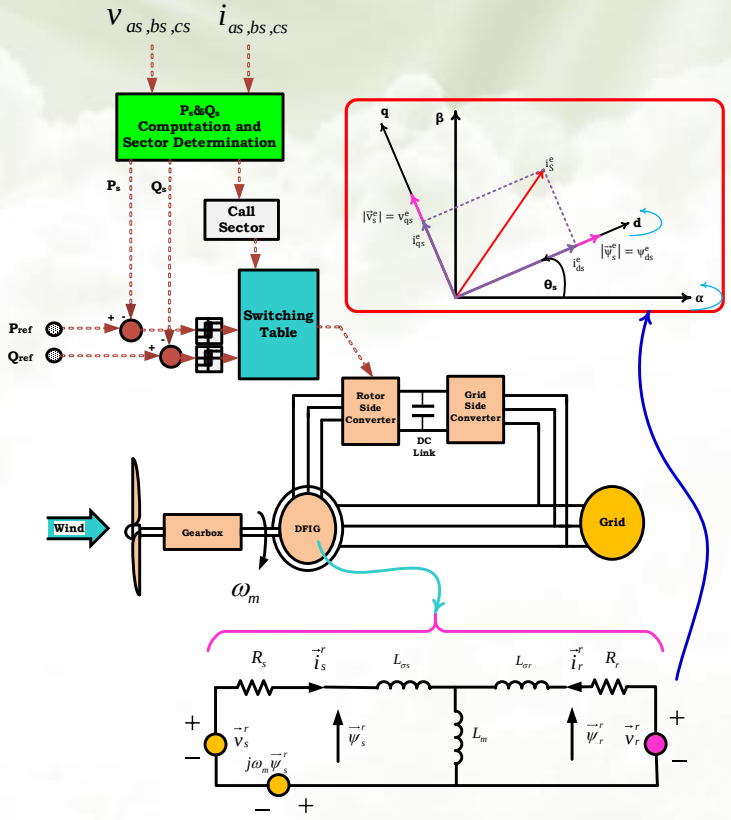

Use your device to scan and read the article online

Citation

M. N. Hashemnia, and A. Dehghan Nayeri, "A New Method for DFIG Control under Unbalanced Grid Voltage Conditions," *Journal of Green Energy Research and Innovation*, vol. 1, no. 4, pp. 86-116, 2024.

https://doi.org/10.61186/jgeri.1.4.86

Online ISSN: 3041-9018

Journal of Green Energy Research and Innovation

Journal Homepage: www.jgeri.araku.ac.ir

A New Method for DFIG Control under Unbalanced Grid Voltage Conditions

Mohammad Naser Hashemnia*, Ali Dehghan Nayeri

Department of Electrical Engineering, Mashhad Branch, Islamic Azad University, Mashhad, Iran.

* ***Corresponding Author:*** *hashemnia@mshdiau.ac.ir*

ARTICLE INFO

Keywords:
Direct power control,
Doubly-fed induction generator,
High selectivity filter,
PI regulator;
Stator flux.

Article history:
Received: 01 February 2024;
Revised: 28 April 2024;
Accepted: 04 May 2024;

Article type:
Research Article

ABSTRACT

This research presents a comprehensive analysis of the performance of direct power control (DPC) for doubly-fed induction generator (DFIG) under both balanced and unbalanced network voltages. Voltage unbalance in three-phase systems results in the presence of positive and negative sequences in both voltages and currents. This unbalance leads to many issues, including active power ripple, reactive power ripple, and an increase in the Total Harmonic Distortion (THD) of the stator current. Therefore, it is crucial to have efficient control of the system to reduce power fluctuations. This research presents two solutions that aim to mitigate the fluctuations in both active and reactive power. The first strategy employs PI regulators within the controller system. A high selectivity filter (HSF) is employed to separate the fundamental component of stator phase currents from the harmonic components. The second option utilizes DPC (Direct Power Control) based on stator flux. The suggested method computes the active and reactive powers that correspond to positive sequence variables. Since grid unbalance has a smaller impact on stator flux compared to stator voltage, it can be demonstrated that the second suggested controller exhibits superior performance to the conventional DPC controller in unbalanced situations. To evaluate the effectiveness of the suggested techniques, a simulation is conducted on a 2MW Doubly-Fed Induction Generator (DFIG) system using the MATLAB/Simulink environment. The results demonstrate that both of the suggested DPC control approaches outperform the conventional DPC controller in terms of control system performance, even under unbalanced situations. Furthermore, these improvements are achieved without significantly increasing the complexity of the control system.

1. Introduction

In recent years, the capacity of installed wind power plants has increased rapidly. Wind energy conversion systems can be classified into two main categories: fixed-speed turbines and variable-speed turbines. Variable-speed turbines operate at or near the point of maximum aerodynamic efficiency. Among the main features of variable speed wind turbines are increased annual energy production due to adaptation of turbine speed to wind speed leading to maximum turbine output power, reduced mechanical stress on

turbine, smooth power injection to network under fault conditions, reduced noise, and higher power quality [1]. Despite the significant benefits of a variable-speed wind turbine, its performance incurs additional expenses. Furthermore, a power electronic converter increases the complexity between the network and the generator. Nevertheless, its utilization is increasing due to its advantageous features. For variable-speed wind turbines, a power electronic converter is used between the wind generator and the grid. Doubly-Fed Induction Generators (DFIGs), permanent magnet synchronous generators, and wound rotor synchronous generators are the most commonly used types of machines in variable speed wind systems. DFIG has numerous advantages over other generators [2] due to its variable speed operation capability and low-cost partial scale converter, among others. Figure 1 shows a DFIG connected to the network. The rotor side converter controls the active and reactive powers of the stator while the grid side converter controls the DC link voltage and the reactive power exchanged.

Despite DFIG's numerous advantages, its primary drawback is that grid disturbances affect the machine due to the stator's direct connection to the grid. If no measures are taken, unbalanced network voltages may result in oscillations in active power, reactive power, and electromagnetic torque [2]. DFIG control methods can be classified into two categories: field-oriented control (FOC) and direct power control (DPC). A wide range of combinations, each with its specific advantages and disadvantages can be utilized [3-9]. Applying direct torque control (DTC) to DFIG in 2002 [9] was a solution to address control drawbacks and simplify PI controller tuning in the vector control method. The DTC control structure consists of an estimation block, hysteresis controllers, and a DTC switching table. The main control variables are the values of electromagnetic torque T_e^* and rotor flux ψ_r^* [9]. Just like the DTC, the DPC was developed over a decade ago primarily for controlling three-phase rectifiers [10]. In the DPC method, the main controlled variables are the stator active power P_s and stator reactive power Q_s [10]. Furthermore, DPC does not require estimation of the control variables as the stator's active and reactive powers may be computed using the stator's voltages and currents. Figure 2 shows the diagram of direct power control.

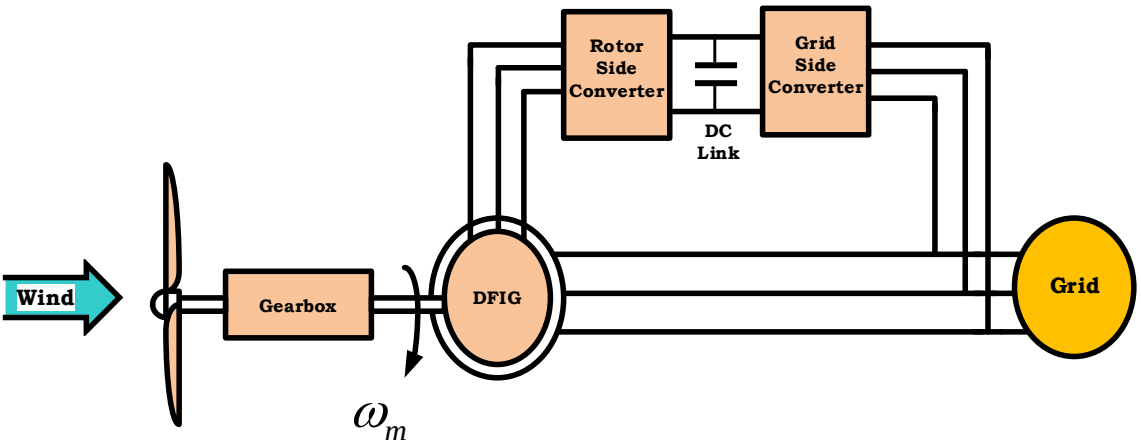

Figure 1. Schematic of a DFIG-based wind turbine connected to the grid.

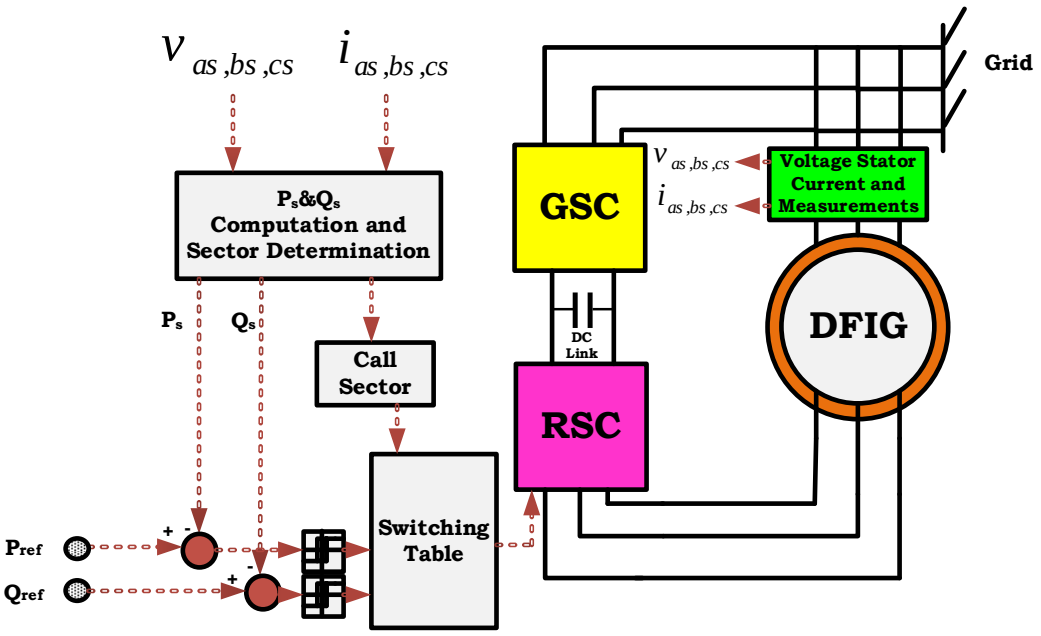

Figure 2. DPC controller structure.

Several researchers have been studying DPC and DTC for DFIG to minimize output ripple and maintain a constant switching frequency on the rotor side converter. These methods include space vector modulation (SVM) [11], discrete space vector modulation technique (DSVM), and predictive direct power control (PDPC) method [12]. All of these approaches have the potential to enhance the performance of DPC but at the cost of increased complexity. Although DPC has a fast response, its main limitation lies in the variable switching frequency. This issue can be resolved by replacing hysteresis controllers with PI controllers or implementing space vector modulation.

A model utilizing predictive control, a subset of space vector modulation, is employed in [12]. This model employs Predictive Direct Power Control (PDPC) to determine active and reactive power errors at the start of the sampling period. Following this phase and upon completion of the sampling time, the active and reactive power errors should be eliminated. Space vector modulation is utilized to generate the necessary switching pulses. The primary drawbacks of PDPC are the online computing issues of microprocessors and the complexity of control.

In [13], the required rotor voltage vectors over a constant period are applied using space vector modulation. Although this method leads to constant switching frequency, the calculation of duty ratios of each voltage vector increases the mathematical computation. Space vector modulation can be performed based on voltage and virtual flux. The DPC controller is characterized by the absence of current loops and the ability to directly control active and reactive powers. The power estimation block is comparable to that of conventional DPC. Direct power control with space vector modulation combines the benefits of direct power control, such as fast dynamic response, with the advantages of vector control, such as a reduced switching frequency. However, the control algorithm's complexity and slower dynamic response compared to direct power control are the main disadvantages of this method. The discrete SVM technique [14] utilizes three rotor voltage

vectors throughout the switching period. These vectors are chosen by the implementation of a modified lookup table and a 5-level hysteresis comparator.

A study is conducted in [15-17] on model predictive DPC (PDPC) control under unbalanced grid voltage conditions. In [15] a low-complexity model predictive control (LC-DPC) based on three voltage vectors is proposed. The results showed that LC-MPDPC can mitigate the current harmonics and reduce power and torque ripples. Reference [16] employs the principle outlined in reference [15]. This paper demonstrates the enhancement of the steady state and dynamic response of the machine by incorporating a second-order generalized integrator (SOGI). Reference [17] utilizes four voltage vectors instead of three, with one voltage vector being applied within a fixed sampling period. In this method, there is no requirement to estimate the rotor flux, and the selection of voltage vector sequences is determined by a straightforward algorithm. While the suggested control strategy exhibits a smoother response under both balanced and unbalanced voltage conditions, it is more complicated compared to previous (PDPC) techniques. A more advanced method for controlling the DFIG in the synchronous reference frame is proposed in [18]. This method is designed to work effectively under both balanced and unbalanced voltage conditions. The direct-resonant method employs a dual-frequency frequency to effectively eliminate negative sequence and harmonic components, resulting in the generation of sinusoidal currents.

The performance is enhanced in [19] through the integration of a disturbance observer and a proportional controller. PI controllers are employed to eliminate the second harmonic oscillatory component of power. Despite the improved power control demonstrated by the simulation results under unbalanced conditions, controller gains must still be adjusted due to the use of PI controllers. On the other hand, the control structure is highly complicated, which necessitates complicated computations and can be quite costly. A proposal was suggested in [20] to integrate vector control and direct torque control to optimize the performance of current, flux, and electromagnetic torque. This approach is preferred over using direct torque control or vector control alone. It ultimately improves the machine's performance in situations where the network is balanced. Compared to the DTC method, the power oscillations are reduced and a smoother response is observed. Compared to the vector control method, it demonstrates a faster dynamic response and reduced dependence on system parameters.

Despite demonstrating enhanced dynamic response and reduced torque and power fluctuations, it still encounters power fluctuations when exposed to unbalanced voltage conditions. In addition, the system utilizes hysteresis controllers leading to a variable switching frequency. Direct power control based on voltage and virtual flux is proposed in [21] for unbalanced voltage and distorted network conditions. By utilizing virtual flux rather than voltage to calculate power, the proposed method eliminates the effect of unbalanced voltage on instantaneous power and, consequently, oscillating active power. However, there are still fluctuations in reactive power.

Two four-switch three-phase converters (FSTPCs) have been implemented in place of two six-switch three-phase converters (SSTPCs) on the rotor and grid side converters

[22]. This method will generate four unbalanced voltage vectors. Three distinct targets are applied to compensate for active and reactive power, electromagnetic torque, and stator current to achieve balance among these four voltage vectors during unbalanced grid voltage conditions. While these objectives result in a reduction of active and reactive power fluctuations, the mitigation of electromagnetic torque variations, and the achievement of balanced stator currents, power oscillations remain. While using FSTPCs lowers costs and switching losses, there are drawbacks to this approach as well. For instance, the voltage gain is decreased for the same rated power, which results in an additional issue. A proposal is made in [23] to combine vector control and direct power control. The combination control method offers the advantages of both vector control and direct power control. The benefits of combining vector and direct power control over the conventional DPC method include a decrease in current THD, enhancement of both active and reactive powers, and fast dynamic response. However, this method exhibits higher THD and power oscillations compared to vector control. Additionally, its performance during voltage dips is deemed unsatisfactory. An investigation was conducted in [24] to study the control of electromagnetic torque and reactive power under unbalanced grid voltage conditions. The study focused on using a stator-flux-oriented reference frame and obtaining the stator flux through an observer. The controller produces sinusoidal currents that are injected into the grid. In the case of an unbalanced grid voltage, the authors of [25] suggest a Voltage Modulated (VM)-DPC approach for DFIGs that makes use of the extended power theory. The absence of sequence extractions causes fluctuations under unbalanced conditions, even though the combination of PI and VM-DPC strategy slightly improves control in normal situations.

A simplified DPC of DFIGs under both normal and unbalanced grid voltage conditions in a stationary reference frame is presented in [26]. This approach offers the advantages of eliminating the decomposition process, axes transformation, and compensation power terms. Stator active and reactive powers are controlled using Vector proportional-integral (VPI) controllers and the performance is compared with proportional-integral-resonant (PIR) controllers through simulations. In [27] a VM-DPC is designed to improve steady-state and transient performances under unbalanced grid voltage conditions. In conjunction with the VM-DPC, a parallel compensator regulates negative-sequence stator current, resulting in improved waveforms for stator current, stator active power, and stator reactive power. For the stator current and voltage, this technique necessitates the extraction of positive and negative sequences. To calculate positive and negative sequences, the authors of [28] devised a mixed integrator, which is a combination of second and third-order integrators. The hysteresis controllers of rotor currents and grid currents generate switching patterns for the rotor side converter and grid side converter, respectively. This method is claimed to possess superior capability in tracking reference currents when compared to the conventional DPC method. Additionally, it eliminates the requirement of tuning eight PI current regulators. A low-complexity model predictive direct power control method is proposed in [29]. This method aims to reduce power ripples and utilizes the extended reactive pq theory. This has decreased the computational

burden of the controller as it now only requires one prediction to determine the voltage vector for the next step. This approach offers several advantages, including the reduction of total harmonic distortion in grid current, fast dynamic response, and robustness to parameter variations.

When it comes to control methods, direct power control offers the fastest dynamic response at the lowest cost. Nevertheless, there are a few downsides to this approach, such as increased power ripples and variable switching frequency. Table 1 represents and compares the performance of the different control methods. Different aspects are considered in this comparison, such as dynamic response, power ripple, dependence on machine parameters, converter switching frequency, computational burden, and cost. Low power ripple and a constant switching frequency characterize the FOC method. In contrast to DPC, however, it has several drawbacks, including a sluggish dynamic response, a heavy dependence on machine parameters, and a greater computational burden. Although direct torque control offers fast dynamic response and minimal dependence on machine parameters, it is not without its limitations, including variable switching frequency and relatively higher power ripples. Both DTC and FOC require measurements of rotor current, which raises the cost of the control system.

High dynamic response and variable switching frequency are typical characteristics of controllers based on switching tables. DPC-SVM combines the advantages of DPC and FOC. DPC-SVM's key features are a constant switching frequency, straightforward implementation, a lower cost compared to alternative controllers, and a low power ripple. Predictive direct power control (P-DPC) has the potential to address the primary challenges associated with DPC. Nevertheless, its implementation is costlier due to the computational burden imposed by the control algorithm's complexity and the requirement for rotor current information. As an alternative to DTC, DPC eliminates the requirement to measure rotor currents, thereby decreasing the cost of control.

Table 1. Comparison of different control methods for DFIG.

Control method	Dynamic response	Power Ripple	Dependence on machine parameters	Switching frequency	Ease of implementation	Output current THD	Cost
FOC	Slow	Low	High	Constant	Complicated	Low	High
DTC	Fast	Very High	Low	Variable	Simple	Normal	High
DPC	Fast	High	Very Low	Variable	Simple	Normal	Low
SVM-DPC	Fast	Low	Low	Constant	Simple	Normal	Low
Predictive	Fast	Low	Very High	Constant	Complicated	Low	High

However, similar to DTC, higher power ripple and variable switching frequency are the primary drawbacks of DPC employing a switching table.

The key contributions of this paper are outlined below:

- Conducting a thorough examination of DFIG performance in the presence of unbalanced grid voltage conditions
- Presenting two strategies aimed at mitigating active and reactive power oscillations
- Introducing a high selectivity filter (HSF) to separate the fundamental component of stator phase currents from the harmonic components
- Demonstrating the effectiveness of the proposed method compared to traditional DPC controllers through extensive simulations

The structure of this paper is as follows: The second section examines the dynamic model of DFIG. Direct power control, various hysteresis band controllers, and switching tables are examined in the third section. The performance of DFIG in an unbalanced voltage condition was addressed in the fourth section. In the fifth section, proposed control approaches are outlined and compared to standard DPC. Finally, in sections six and seven, the simulation findings and conclusions are presented.

2. Structure and Dynamic Modeling of DFIG

Given the presence of feedback loops in the DFIG control system, it is important to take into account its dynamic behavior. DFIG control methods, such as DPC and FOC, are discussed using a two-axis model. The DFIG equivalent circuit can be defined in various reference frames, including the stator reference frame, rotor reference frame, and synchronous reference frame [30]. The rotor voltage equations are written in the rotor (natural) reference frame since the DFIG is controlled from the rotor side by the rotor side converter. The DFIG equivalent circuit in the rotor reference frame is depicted in Figure 3. It is important to mention that the model neglects saturation and core loss effects. Additionally, the grid is simplified as a pure voltage source, meaning the internal Thévenin impedance of the grid is not taken into account.

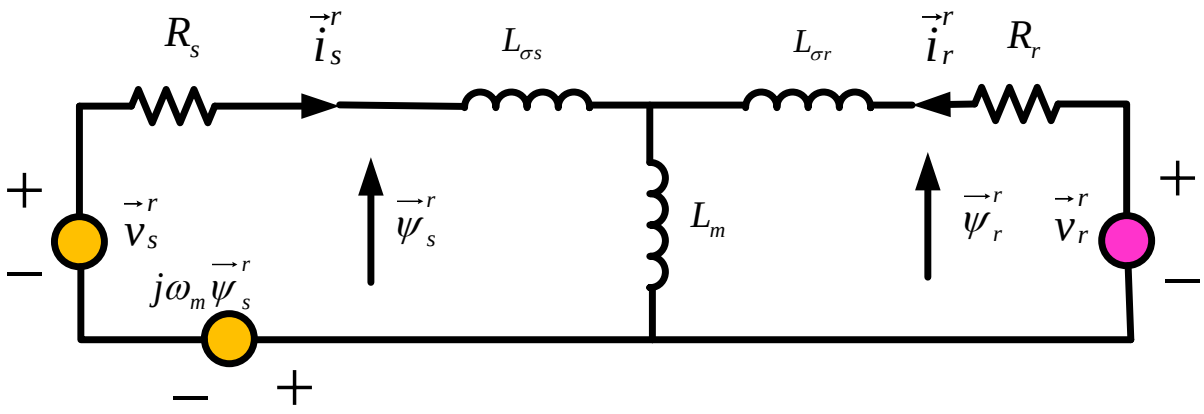

Figure 3. DFIG equivalent circuit in the rotor reference frame [30].

3. Conventional Direct Power Control Principles

Referring to Figure 3, the stator active and reactive power expressions can be derived in the rotor reference frame. Active power consumed and reactive power injected by the stator of the machine are taken to be positive [31]. Accordingly, the input active power of the stator from the network side, neglecting the stator resistance, is as follows:

$$P_s = \frac{3}{2}\mathrm{Re}\{(\dot{\vec{\psi}}_s^r + j\omega_m \vec{\psi}_s^r)\cdot \vec{i}_s^{r*}\} \tag{1}$$

Similarly, the output reactive power is calculated as follows:

$$Q_s = -\frac{3}{2}\mathrm{Im}\{(\dot{\vec{\psi}}_s^r + j\omega_m \vec{\psi}_s^r).\vec{i}_s^{r*}\} \tag{2}$$

The relative position of the stator and rotor flux space vectors in the rotor reference frame is shown in Figure 4, where θ_ψ is the spacial angle between the stator and rotor flux space vectors.

As shown in Appendix A, Equation (1) and (2), can be rewritten as follows:

$$P_s = -\frac{3}{2}\frac{L_m}{\sigma L_s L_r}\omega_s \left|\vec{\psi}_s^r\right|\left|\vec{\psi}_r^r\right|\sin\theta_\psi \tag{3}$$

$$Q_s = \frac{3}{2}\frac{\omega_s}{\sigma L_s}\left|\vec{\psi}_s^r\right|\left(\frac{L_m}{L_r}\left|\vec{\psi}_r^r\right|\cos\theta_\psi - \left|\vec{\psi}_s^r\right|\right) \tag{4}$$

Since there is a direct connection to the network, which is assumed to have a positive sequence only in this case, the magnitude of the stator flux space vector can be taken to be constant. The time derivatives of Eqauation (3) and (4) then yield:

$$\begin{aligned}\frac{dP_s}{dt} &= -\frac{3}{2}\frac{L_m}{\sigma L_s L_r}\omega_s \left|\vec{\psi}_s^r\right|\frac{d(\left|\vec{\psi}_r^r\right|\sin\theta_\psi)}{dt}\\ \frac{dQ_s}{dt} &= \frac{3}{2}\frac{L_m}{\sigma L_s L_r}\omega_s \left|\vec{\psi}_s^r\right|\frac{d(\left|\vec{\psi}_r^r\right|\cos\theta_\psi)}{dt}\end{aligned} \tag{5}$$

Therefore, fast changes in active and reactive powers are possible with corresponding changes in $\left|\vec{\psi}_r^r\right|\sin\theta_\psi$ and $\left|\vec{\psi}_r^r\right|\cos\theta_\psi$, respectively. In Figure 4, $\left|\vec{\psi}_r^r\right|\sin\theta_\psi$ and $\left|\vec{\psi}_r^r\right|\cos\theta_\psi$ represent, respectively, the components of the rotor flux perpendicular and in the direction of stator flux space vector.

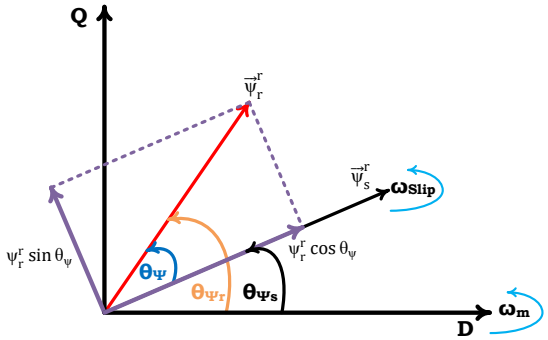

Figure 4. Stator and rotor flux space vectors in rotor reference frame [31].

Therefore, if the rotor flux changes in the direction of the stator flux space vector, then $\left|\vec{\psi}_r^r\right|\cos\theta_\psi$ and accordingly the stator reactive power Q_s changes; on the other hand, the change in rotor flux space vector is perpendicular to the stator flux, then $\left|\vec{\psi}_r^r\right|\sin\theta_\psi$ and stator active power P_s is modified.

The rotor side converter is a three-phase voltage source converter with two switches for each leg. In Figure 5, S_a, S_b and S_c represent the switching functions of every leg of the inverter. If the upper switches are connected, the positive DC voltage is applied, and if the lower switches are connected the applied voltage will be zero.

According to the combination of switching states, two null vectors (V_0,V_7) and six active vectors ($V_1 - V_6$) can be generated. By neglecting the voltage drop on the rotor resistance, the rotor voltage equation in its natural reference frame can be expressed as follows in Equation (6) [31]:

$$\vec{v}_r^r = R_r\vec{i}_r^r + \frac{d\vec{\psi}_r^r}{dt} \cong \frac{d\vec{\psi}_r^r}{dt} \tag{6}$$

The above expression shows that the rotor flux vector moves in the direction of the voltage vector applied to the rotor and its velocity is proportional to the magnitude of the applied voltage vector. It is thus possible to adjust the rotor flux velocity by choosing appropriate voltage vectors.

Figure 6 shows the stator flux and rotor flux space vectors in a rotating plane attached to the rotor with eight possible rotor voltage vectors. If the position of the stator flux is known, the effect of using $\left|\vec{\psi}_r^r\right|\sin\theta_\psi$ and $\left|\vec{\psi}_r^r\right|\cos\theta_\psi$ can be determined for each voltage vector. Figure 7 shows the initial position of rotor flux at moment t_1 and the final position of rotor flux at moment $t_1 + \Delta t$, assuming that the rotor flux is located in the first sector of the rotor reference frame. It may be noted that $\vec{\psi}_r^r$ is drawn ahead of $\vec{\psi}_s^r$ as the generating mode of operation has been considered.

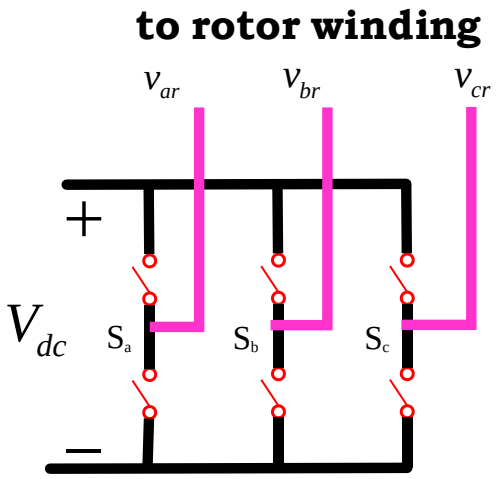

Figure 5. Schematic of a rotor-side VSI.

Using $\vec{v}_2$ and $\vec{v}_6$ leads to the increase of the final rotor flux and increases the stator-generated active power. Using $\vec{v}_1$ and $\vec{v}_5$ leads to the decrease of the final rotor flux and decreases the stator-generated active power. Using $\vec{v}_3$ and $\vec{v}_4$ does not affect the stator active power.

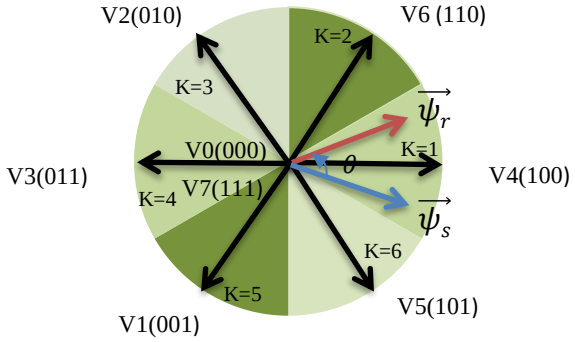

Figure 6. Voltage space vectors applied to the converter.

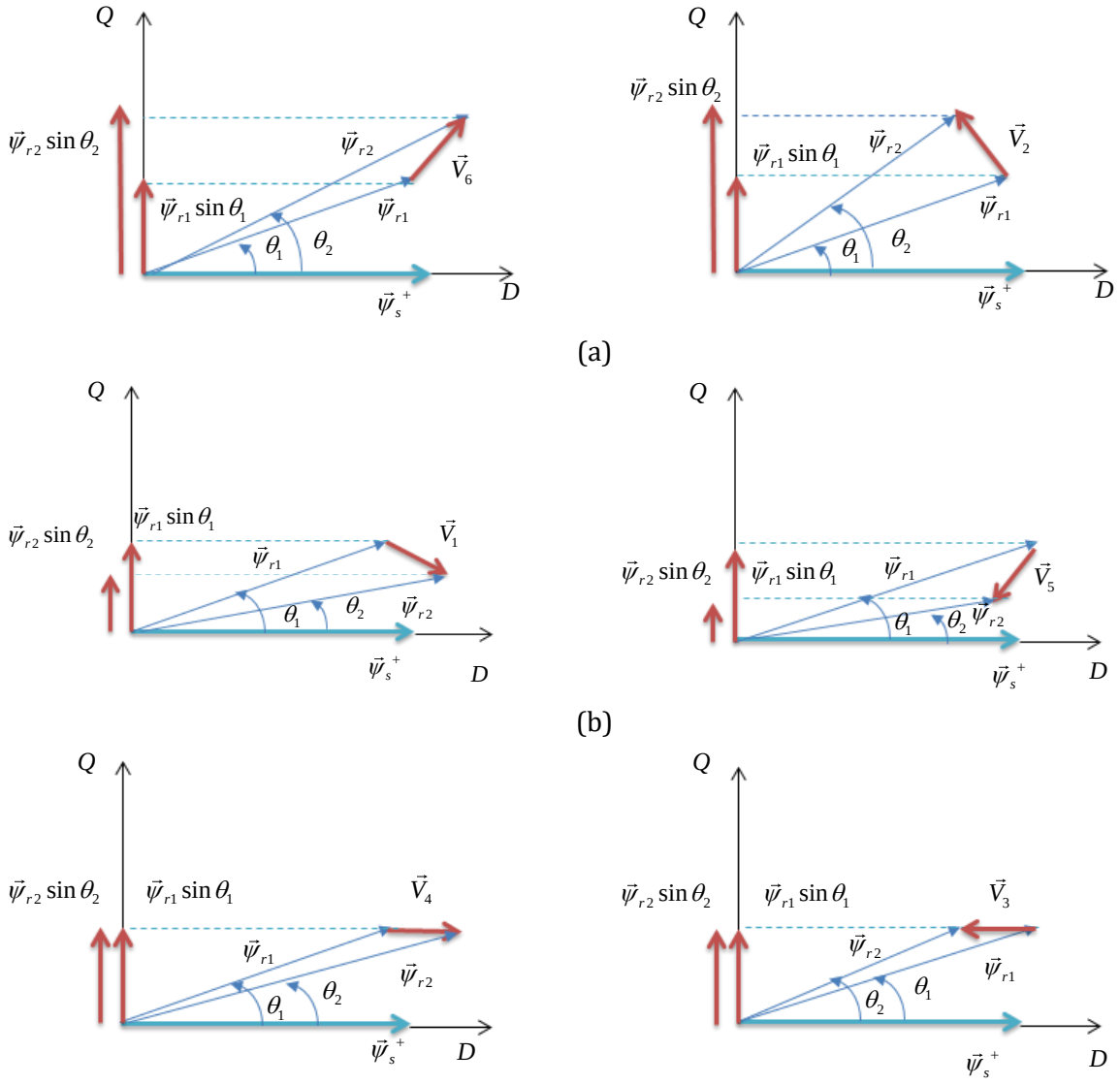

Figure 7. Effect of active vectors on active power, a: $\vec{v}_2$ and$\vec{v}_6$,b: $\vec{v}_1$ and $\vec{v}_5$, c: $\vec{v}_3$ and $\vec{v}_4$.

Table 2. Effect of voltage vectors on stator input active power and output reactive power.

K=1, 2, 3, .., 6	v_{k-2}	v_{k-1}	v_k	v_{k+1}	v_{k+2}	v_{k+3}
P_s	↑	↓	↑	↓	↓↑	↓↑
Q_s	↑	↑	↓	↓	↓	↑

Table 2 illustrates the effect of different voltage vectors on active and reactive powers. The angle between the stator flux and rotor flux may increase or decrease by applying a zero-vector depending on the operating mode of the machine. For sub-synchronous mode, the stator flux movement reduces the angle between the rotor flux and the stator flux ($\theta_2 < \theta_1$), which causes active power reduction and reactive power increment. In other cases, the stator flux movement increases the angle between the rotor and the stator flux ($\theta_2 > \theta_1$), which causes active power increment and reactive power reduction.

3.1. Flux estimation methods

Multiple techniques exist for determining the position of the rotor flow vector. The estimation of the rotor and stator flux is performed by incorporating the rotor angular position in [32]. One drawback of this technology is its dependence on rotor currents. Machine parameters are required to calculate flux, which reduces the speed of estimation and adds to the complexity of the control. This approach provides a more precise estimation of the angle of flux.

An alternative approach for determining the rotor flux angle involves utilizing the stator flux. The stator voltage is utilized in [31] to determine the stator flux angle. This approach assumes a small angle between the stator and rotor flux and considers the position of the rotor and stator flux inside the same sector. The stator flux is estimated in the stator reference frame by integrating the stator voltage while neglecting the stator resistance. This method can accurately estimate the stator flux due to the harmonic-free and constant frequency nature of the stator voltage. Integration is typically implemented by employing a low pass filter in practical applications.

In this work, the rotor flux angle is estimated using the stator flux. The voltage vector applied to the rotor windings is determined by the position of the rotor flux and the different active and reactive power states.

3.2. Direct Active and Reactive Power Control

In this section, the computed active and reactive powers are compared to their respective reference values, resulting in the generation of error signals, fed to two hysteresis comparators. Two-level, three-level, or four-level hysteresis controllers can be used which yield different switching tables for control of the rotor side converter. In [33],

a two-level hysteresis controller for active and reactive powers is used. In [34] a three-level controller is used for active power:

$$\begin{aligned} &P_{ref} \geq P + \Delta P \rightarrow dp = 1 \\ &P_{ref} \leq P - \Delta P \rightarrow dp = -1 \\ &P_{ref} \leq P - \Delta \mathrm{P} \quad or \quad P_{ref} \geq P + \Delta P \rightarrow dp = 0 \end{aligned} \tag{7}$$

and a two-level controller is used for reactive power, as:

$$\begin{aligned} &Q_{ref} \geq Q + \Delta Q \rightarrow dq = 1 \\ &Q_{ref} \leq Q - \Delta Q \rightarrow dq = -1 \end{aligned} \tag{8}$$

In Equation (7) and (8), ΔP and ΔQ represent the hysteresis bandwidth. The values 1/-1 indicate the need to increase/decrease stator active and reactive powers to approach the reference value.

A three-level hysteresis controller is employed in [31] to regulate both active and reactive powers. The three-level controller incorporates a greater number of switching states, resulting in improved accuracy of the control system for active and reactive power regulation.

A study was undertaken in [35,36] to investigate the impact of active and reactive power hysteresis bands on the performance of DPC drives. The study reveals that the hysteresis band has a significant influence on the THD of the stator current and the oscillations in the control system. The study conducted in [37] found that a narrower hysteresis band leads to an increase in switching frequency. Alternatively, when the hysteresis band is increased to 25% of rated power, the switching frequency decreases to 500 Hz. Therefore, by utilizing the output signals of hysteresis comparators (S_p and S_q) in conjunction with the angular information of the rotor flux space vector, an optimal switching table is created.

3.3. The effect of different switching tables

For a long time, switching table designs for DPC and DTC have been of interest. In [38-43], the differences between various switching tables are examined and reviewed. Since the majority of researchers have focused on analyzing DPC performance under balanced network voltage, the development of switching tables has primarily been done under this specific condition. The initial switching table developed by Noguchi is currently regarded as a standard for evaluating other tables [44]. This table exhibits significant fluctuations in both active and reactive power as a result of an incorrect choice of voltage vectors [38]. Later on, Malinowski introduced a new table for three-phase rectifiers [45]. Utilizing zero vectors in this table mitigates power fluctuations and enhances the performance of the control system. Researchers subsequently introduced novel switching tables. New tables significantly enhanced the dynamic and steady-state performance of the DPC in comparison to conventional tables by suppressing active and reactive power fluctuations more effectively [21]. One of the reasons that reactive power error in some tables was overlooked is due to the higher priority given to reducing ripple for active power [21]. In

general, the switching tables are classified according to their accuracy in power regulation, the amount of active power ripple, the current THD, the switching frequency, and the response time. In [40], a study is conducted on a switching table that utilizes active vectors. In this table, the elimination of zero vectors is based on their negligible impact on active and reactive powers. While this switching table has led to a faster response time, it has also caused an increase in power ripple, current THD, and switching frequency.

In this paper, a three-level hysteresis comparator is utilized for both active and reactive powers. A switching table of 54 different entries for voltage vectors is employed, as per the reference [31], which is presented in Table 3. Zero voltage vectors are utilized when there are no errors in both active and reactive power.

4. Performance Analysis under Unbalanced Voltage Conditions

Supplying DFIG with unbalanced grid voltage can have detrimental effects on its performance. These effects include increased losses, reduced efficiency and torque, and higher machine temperatures with uneven distribution [46]. The intensity of these effects is directly influenced by the severity of the unbalanced voltage in the machine terminals. For this reason, control system performance is crucial. Under unbalanced network conditions, three-phase quantities like voltage, current, and flux are separated into positive and negative sequence components by ignoring the zero sequence.

In [47], voltage, current, and flux in the stator reference frame have been separated into positive and negative sequence components as follows in Equation (9):

$$\vec{F}_{\alpha\beta}(t) = \vec{F}_{\alpha\beta+}(t) + \vec{F}_{\alpha\beta-}(t) = \left|\vec{F}_{\alpha\beta+}\right|.e^{j(\omega_s t+\varphi_+)} + \left|\vec{F}_{\alpha\beta-}\right|.e^{-j(\omega_s t+\varphi_-)} \quad (9)$$

where φ_+ and φ_- are phase shifts related to the positive and negative components. As shown in Figure 8, in the dq^+ reference frame, the d^+ axis is fixed to the positive voltage vector rotating at the speed of ω_s. For dq^- reference frame, the d^- axis rotates at the opposite direction at the speed of $-\omega_s$ and its phase angle related to the α axis is $-\theta_s$ [45].

Table 3. Switching Table for the DPC [31].

S_p	S_q	I	II	III	IV	V	VI
1	1	V_5	V_4	V_6	V_2	V_3	V_1
	0	V_4	V_6	V_2	V_3	V_1	V_5
	-1	V_6	V_2	V_3	V_1	V_5	V_4
0	1	V_1	V_5	V_4	V_6	V_2	V_3
	0	V_0, V_7	V_0, V_7	V_0, V_7	V_0, V_7	V_0, V_7	V_0, V_7
	-1	V_2	V_3	V_1	V_5	V_4	V_6
-1	1	V_1	V_5	V_4	V_6	V_2	V_3
	0	V_3	V_1	V_5	V_4	V_6	V_2
	-1	V_2	V_3	V_1	V_5	V_4	V_6

According to Figure 8, the transformation rules between $\alpha\beta$, dq^+ and dq^- reference frames are as follows in Equation (10):

$$\vec{F}_{dq}^{+} = \vec{F}_{\alpha\beta}.e^{-j\omega_s t},\ \vec{F}_{dq}^{-} = \vec{F}_{\alpha\beta}.e^{+j\omega_s t} \tag{10}$$

$$\vec{F}_{dq}^{+} = \vec{F}_{dq}^{-}.e^{-j2\omega_s t},\ \vec{F}_{dq}^{-} = \vec{F}_{dq}^{+}.e^{+j2\omega_s t} \tag{11}$$

F variables can be expressed as positive and negative sequence components [46]:

$$\vec{F}_{dq}^{+} = \vec{F}_{dq+}^{+} + \vec{F}_{dq-}^{+} + \vec{F}_{dq5-}^{+} + \vec{F}_{dq7+}^{+} \tag{12}$$

According to Equation (12), under unbalanced and distorted grid voltage, variable F consists of 5 and 7 harmonics, which rotate in the dq reference frame. In Equation (12), the superscripts "+" and "-" refer to the positive and negative reference frames, and the subscripts "+" and "-" refer to the positive and negative sequence components. Using Equation (11), Equation (12) can also be written as:

$$\vec{F}_{dq}^{+} = \vec{F}_{dq+}^{+} + \vec{F}_{dq-}^{-}e^{-2j\omega_s t} + \vec{F}_{dq5-}^{5-}e^{-6j\omega_s t} + \vec{F}_{dq7+}^{7+}e^{+6j\omega_s t} \tag{13}$$

As shown in Equation (13), in the dq^+ reference frame, F contains a dc term and oscillating components. As a result, Equation (13) can be represented as Equation (14):

$$\begin{aligned} \vec{F}_{d}^{+} &= \vec{F}_{d+}^{+} + \vec{F}_{d-}^{+} \\ \vec{F}_{q}^{+} &= \vec{F}_{q+}^{+} + \vec{F}_{q-}^{+} \end{aligned} \tag{14}$$

where:

$$\begin{aligned} \vec{F}_{d-}^{+} &= (\vec{F}_{d-}^{-}\cos 2\omega_s t + \vec{F}_{q-}^{-}\sin 2\omega_s t) + (\vec{F}_{d5-}^{5-}\cos 6\omega_s t + \vec{F}_{q5-}^{5-}\sin 6\omega_s t) + (\vec{F}_{d7}^{7}\cos 6\omega_s t - \vec{F}_{q7}^{7}\sin 6\omega_s t) \\ \vec{F}_{q-}^{+} &= (\vec{F}_{q-}^{-}\cos 2\omega_s t - \vec{F}_{d-}^{-}\sin 2\omega_s t) + (\vec{F}_{q5-}^{5-}\cos 6\omega_s t - \vec{F}_{d5-}^{5-}\sin 6\omega_s t) + (\vec{F}_{q7}^{7}\cos 6\omega_s t + \vec{F}_{d7}^{7}\sin 6\omega_s t) \end{aligned} \tag{15}$$

Therefore, stator voltage and current in the dq^+ reference frame, neglecting 5 and 7 harmonics, are as follows:

$$\begin{aligned} \vec{v}_{sdq}^{+} &= \vec{v}_{sdq+}^{+} + \vec{v}_{sdq-}^{-}e^{-2j\omega_s t} \\ \vec{i}_{sdq}^{+} &= \vec{i}_{sdq+}^{+} + \vec{i}_{sdq-}^{-}e^{-2j\omega_s t} \end{aligned} \tag{16}$$

Power relations are written as follows:

$$\begin{aligned} \begin{bmatrix} P \\ Q \end{bmatrix} = \begin{bmatrix} \overline{P} + \tilde{P} \\ \overline{Q} + \tilde{Q} \end{bmatrix} &= \frac{3}{2}\begin{bmatrix} \vec{v}_{d+}^{+}\vec{i}_{d+}^{+} + \vec{v}_{q+}^{+}\vec{i}_{q+}^{+} + \vec{v}_{d-}^{-}\vec{i}_{d-}^{-} + \vec{v}_{q-}^{-}\vec{i}_{q-}^{-} \\ \vec{v}_{q+}^{+}\vec{i}_{d+}^{+} - \vec{v}_{d+}^{+}\vec{i}_{q+}^{+} + \vec{v}_{q-}^{-}\vec{i}_{d-}^{-} - \vec{v}_{d-}^{-}\vec{i}_{q-}^{-} \end{bmatrix} \\ &+ \frac{3}{2}\begin{bmatrix} \vec{v}_{d-}^{+}\vec{i}_{d+}^{+} + \vec{v}_{q-}^{+}\vec{i}_{q+}^{+} + \vec{v}_{d+}^{+}\vec{i}_{d-}^{+} + \vec{v}_{q+}^{+}\vec{i}_{q-}^{+} \\ \vec{v}_{q-}^{+}\vec{i}_{d+}^{+} - \vec{v}_{d-}^{+}\vec{i}_{q+}^{+} + \vec{v}_{q+}^{+}\vec{i}_{d-}^{+} - \vec{v}_{d+}^{+}\vec{i}_{q-}^{+} \end{bmatrix} \end{aligned} \tag{17}$$

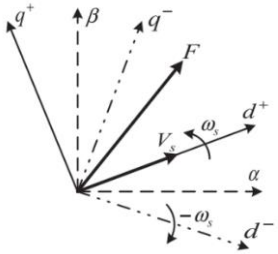

Figure 8. Relation between $\boldsymbol{dq^+}$ and $\boldsymbol{dq^-}$ reference frames [47].

The oscillating components of active and reactive power cause DC link voltage and electromagnetic torque ripples. To minimize these ripples, the oscillating terms of active and reactive powers in Equation (17) should be zero, as shown below in Equation (18):

$$\begin{bmatrix} \overline{P} \\ \overline{Q} \\ 0 \\ 0 \end{bmatrix} = \frac{3}{2} \begin{bmatrix} \vec{v}_{d+}^{+}\vec{i}_{d+}^{+} + \vec{v}_{q+}^{+}\vec{i}_{q+}^{+} + \vec{v}_{d-}^{-}\vec{i}_{d-}^{-} + \vec{v}_{q-}^{-}\vec{i}_{q-}^{-} \\ \vec{v}_{q+}^{+}\vec{i}_{d+}^{+} - \vec{v}_{d+}^{+}\vec{i}_{q+}^{+} + \vec{v}_{q-}^{-}\vec{i}_{d-}^{-} - \vec{v}_{d-}^{-}\vec{i}_{q-}^{-} \\ \vec{v}_{d\square}^{+}\vec{i}_{d+}^{+} + \vec{v}_{q\square}^{+}\vec{i}_{q+}^{+} + \vec{v}_{d+}^{+}\vec{i}_{d\square}^{+} + \vec{v}_{q+}^{+}\vec{i}_{q\square}^{+} \\ \vec{v}_{q\square}^{+}\vec{i}_{d+}^{+} - \vec{v}_{d\square}^{+}\vec{i}_{q+}^{+} + \vec{v}_{q-}^{-}\vec{i}_{d\square}^{-} - \vec{v}_{d-}^{-}\vec{i}_{q\square}^{-} \end{bmatrix} \tag{18}$$

Consequently, active and reactive powers can be written as follows in Equation (19):

$$P = \overline{P} + \tilde{P} \qquad Q = \overline{Q} + \tilde{Q} \tag{19}$$

As mentioned before, $\vec{v}_{dq+}^{+}$, $\vec{i}_{dq+}^{+}$, $\vec{v}_{dq-}^{-}$ and $\vec{i}_{dq-}^{-}$ are DC terms while $\vec{v}_{dq\sim}^{+}$ and $\vec{i}_{dq\sim}^{+}$ are oscillating terms with frequency of $2\omega_s$. Constant power terms ($\overline{P}$ and $\overline{Q}$) are due to the interaction between constant components of voltage and current in the synchronous frames. It should be noted that the 5th and 7th harmonics of the grid voltage have been neglected in this paper for the sake of simplicity.

5. Improving DFIG performance under unbalanced conditions

DFIG voltage and flux equations are written in the rotor reference frame concerning Figure 4 as follows:

$$\vec{v}_s^{\,r} = R_s\vec{i}_s^{\,r} + \frac{d\vec{\psi}_s^{\,r}}{dt} + j\omega_m\vec{\psi}_s^{\,r} \qquad \vec{v}_r^{\,r} = R_r\vec{i}_r^{\,r} + \frac{d\vec{\psi}_r^{\,r}}{dt} \tag{20}$$

$$\vec{\psi}_r^{\,r} = L_r\vec{i}_r^{\,r} + L_m\vec{i}_s^{\,r} \qquad \vec{\psi}_s^{\,r} = L_s\vec{i}_s^{\,r} + L_m\vec{i}_r^{\,r} \tag{21}$$

Since the stator side is connected to the grid and the stator voltage is unbalanced, Equation (20) and (21) also include the positive and negative sequence components. Therefore, stator active and reactive powers take the following form:

$$P_s = \overline{P_s} + \tilde{P}_s \qquad Q_s = \overline{Q_s} + \tilde{Q}_s \tag{22}$$

Equation (22) shows that the stator power under unbalanced conditions has DC and oscillating components. Our strategy in this paper is to reduce the oscillation of active and reactive powers of the rotor side converter under unbalanced voltage conditions. In this paper, two strategies are proposed to mitigate the effect of unbalanced voltage on active and reactive power ripples.

One method to detect and isolate harmonic components of current is the so-called instantaneous power p–q theory [47,48]. In this method, harmonics from the load currents are extracted by the computation of instantaneous power and using (HPF) and/or (LPF). This method is no longer used because of the complex computation of voltage and current. A more common method is described in [49]. In this method, only the currents are measured and the harmonic part is extracted. The main problem in this scheme is the lack of selective harmonic detection because of using (LPF) [50]. In [51] a

new time-domain harmonic detection method was proposed based on (HSF). This method requires current measurement and isolates a particular harmonic or separates the harmonic components from the fundamental component and current references can be calculated. In this paper, we propose (HSF) instead of conventional (LPF) to extract the fundamental component of stator current.

5.1. Direct power control with PI regulator

This section will address the implementation of direct power control with a PI regulator in the presence of unbalanced conditions. The simulation findings demonstrate that while the proposed method introduces complexity to the control system structure compared to the conventional DPC method, it effectively reduces power ripple in the presence of unbalanced voltage conditions. The controller structure is shown in Figure 9. In the first step, active and reactive powers are compared with their respective reference values, and calculated errors are passed to the PI controller. The output signals are considered as reference values for stator or rotor currents. To calculate rotor currents in the dq^+ reference frame, rotor currents should first be transformed to the synchronous reference frame. A PLL is used to calculate the reference frame angle. Instead of the rotor currents, stator currents can be used in the positive synchronous reference frame. In this case, only the angle of the positive sequence stator current (θ_s^+) is estimated using PLL. After comparison of the stator currents with their reference values, the outputs are given to hysteresis comparators. Similar to the conventional DPC method, the output signals from two hysteresis comparators are applied to the switching table to select the appropriate voltage vector. As mentioned before under unbalanced voltage conditions the stator current contains fundamental and harmonic components, that is:

$$\vec{i}_{sdq}^{+} = \vec{i}_{sdq+}^{+} + \vec{i}_{sdq-}^{-} e^{-2j\omega_s t} + \vec{i}_{sdq5-}^{5-} e^{-6j\omega_s t} + \vec{i}_{sdq7+}^{7+} e^{+6j\omega_s t} \quad (23)$$

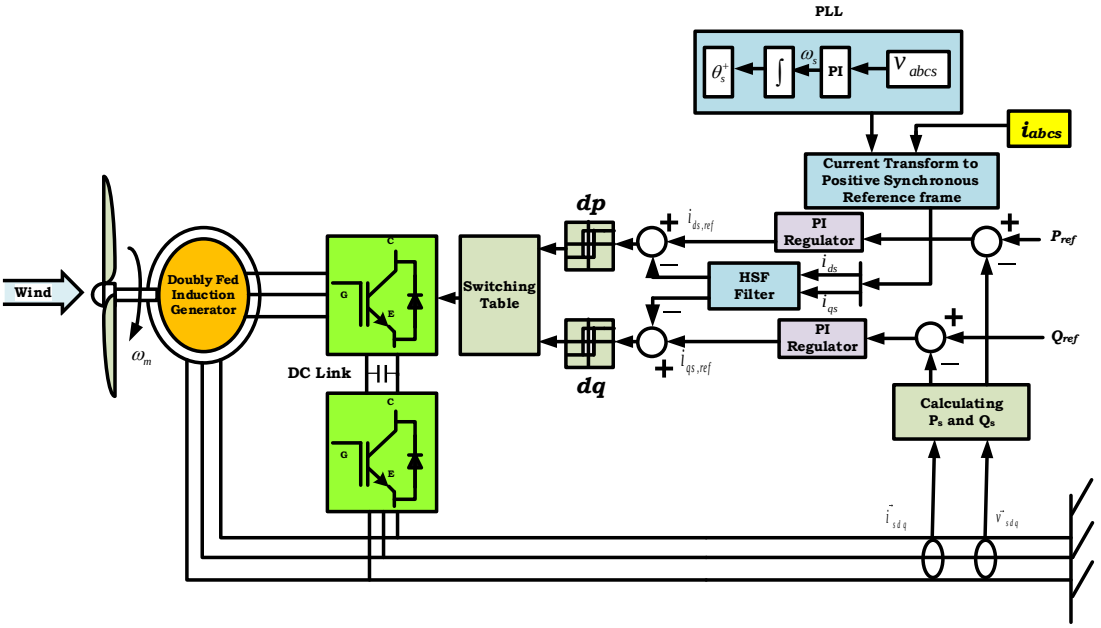

Figure 9. Structure of DPC with PI regulator under unbalanced grid voltage conditions.

In Equation (23) $\vec{i}^{+}_{sdq+}$, $\vec{i}^{-}_{sdq-}$, $\vec{i}^{5-}_{sdq5-}$ and $\vec{i}^{7+}_{sdq7+}$ are DC values. This means that the stator currents in the dq^{+} reference frame include DC and oscillating components. The HSF filter only passes the DC component in the positive synchronous frame ($\vec{i}^{+}_{sdq+}$); therefore, in this control method, the reference d and q stator currents are directly compared with corresponding DC components generated by the HSF filter. The details of the proposed filter are given in the following.

5.1.1. High selectivity filter (HSF)

A high selectivity filter (HSF) is used to separate the fundamental component of the signal instead of conventional (LPF) and (HPF) filters. Hong-sock Song in [52] shows that the integral in the synchronous reference frame is given as Equation (24):

$$V_{xy}(t) = e^{j\omega_s t}\int e^{-j\omega_s t}U_{xy}(t)dt \tag{24}$$

Where U_{xy} and V_{xy} are the instantaneous signals, before and after integration in the synchronous reference frame, respectively. Equation (24) can be expressed by the following transfer function after Laplace transformation:

$$H(s) = \frac{V_{xy}(s)}{U_{xy}(s)} = \frac{s + j\omega_s}{s^2 + \omega_s^2} \tag{25}$$

In Equation (25), constant K is introduced in the transfer function $H(s)$, to obtain an HSF with a cut-off frequency. So, the previous transfer function becomes:

$$H(s) = \frac{V_{xy}(s)}{U_{xy}(s)} = k\frac{(s+k) + j\omega c}{(s+k)^2 + \omega_c^2} \tag{26}$$

Replacing $V_{xy}(s)$ with X_{dq} and $U_{xy}(s)$ with $\hat{X}_{dq}$, Equation (26) is rewritten as Equation (27):

$$\begin{aligned}\hat{X}_d(s) &= \frac{k(s+k)}{(s+k)^2 + \omega_c^2}X_d(s) - \frac{k\omega_c}{(s+k)^2 + \omega_c^2}X_q(s)\\ \hat{X}_q(s) &= -\frac{k\omega_c}{(s+k)^2 + \omega_c^2}X_d(s) + \frac{k(s+k)}{(s+k)^2 + \omega_c^2}X_q(s)\end{aligned} \tag{27}$$

Where X can be current or voltage. Therefore, the above equation is written as Equation (28):

$$\begin{aligned}\hat{X}_d(s) &= \frac{k}{s}[X_d(s) - \hat{X}_d(s)] - \frac{\omega_c}{s}\hat{X}_q(s)\\ \hat{X}_q(s) &= \frac{k}{s}[X_q(s) - \hat{X}_q(s)] - \frac{\omega_c}{s}\hat{X}_d(s)\end{aligned} \tag{28}$$

The (HSF) block diagram for the separation of the fundamental component ($\hat{X}_{dq}$) from X_{dq} in the synchronous reference frame is shown in Figure 10. In this paper, we consider k=40 for good dynamic response.

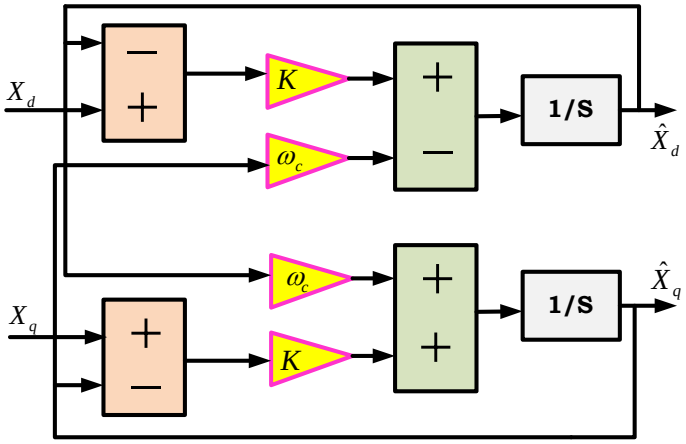

Figure 10. The block diagram of the HSF filter [52].

5.2. DPC using stator flux

In this section, the calculation of stator active and reactive powers in terms of stator flux is discussed. The relation between stator voltage and stator flux in the synchronous reference frame is shown in Figure 11 [53]. The stator apparent power can be expressed in terms of quantities in the stationary reference frame as follows:

$$S_s = \frac{3}{2}\vec{v}_s^{\,s}\vec{i}_s^{\,s^*} \tag{29}$$

According to the stator voltage equation in the stationary reference frame, if stator resistance losses are neglected, the flux and voltage can be related as follows:

$$\vec{v}_s^{\,s} = \frac{d}{dt}\vec{\psi}_s^{\,s} \tag{30}$$

$$\vec{\psi}_s^{\,s} = \vec{\psi}_s^{\,e} e^{j\omega_s t} \tag{31}$$

$$\frac{d}{dt}\vec{\psi}_s^{\,s} = j\omega_s \vec{\psi}_s^{\,e} e^{j\omega_s t} \tag{32}$$

Substitution of Equation (31) and Equation (32) in Equation (29), yields:

$$S_s = \frac{3}{2}\vec{v}_s^{\,s}\vec{i}_s^{\,s^*} = \frac{3}{2}\{(\dot{\vec{\psi}}_s^{\,s})\cdot\vec{i}_s^{\,s}\} = \frac{3}{2}\{(\dot{\vec{\psi}}_s^{\,e}e^{j\omega_s t})\cdot(\vec{i}_s^{\,e}e^{j\omega_s t})^*\} = \frac{3}{2}\{(\dot{\vec{\psi}}_s^{\,e}e^{j\omega_s t} + j\omega\vec{\psi}_s^{\,e}e^{j\omega_s t})\cdot(\vec{i}_s^{\,e}e^{j\omega_s t})^*\} \tag{33}$$

More manipulation of Equation (33) gives:

$$\begin{aligned} S_s &= \frac{3}{2}\{((\dot{\psi}_{ds} + j\dot{\psi}_{qs})e^{j\omega_s t} + j\omega_s(\psi_{ds} + j\psi_{qs}))e^{j\omega_s t})\cdot((i_{ds} + ji_{qs}))e^{j\omega_s t})^*\} \\ &= \frac{3}{2}\{e^{j\omega_s t}(\dot{\psi}_{ds} + j\dot{\psi}_{qs}) + j\omega_s\psi_{ds} - \omega_s\psi_{qs}))((i_{ds} - ji_{qs}))e^{-j\omega_s t})\} \end{aligned} \tag{34}$$

Further simplification yields:

$$S_s = \frac{3}{2}(\dot{\psi}_{ds}i_{ds} + \dot{\psi}_{qs}i_{qs} - \omega_s\psi_{qs}i_{ds} + \omega_s\psi_{ds}i_{qs} - j\dot{\psi}_{ds}i_{qs} + \dot{\psi}_{qs}i_{ds} + j\omega_s\psi_{qs}i_{qs} + j\omega_s\psi_{ds}i_{ds}) \tag{35}$$

In the above equation, terms containing derivatives are neglected because they are constant in the synchronous reference frame. Thus, Equation (35) is simplified as follows:

$$S_s = \frac{3}{2}\{-\omega_s\psi_{qs}i_{ds} + \omega_s\psi_{ds}i_{qs} + j(\omega_s\psi_{qs}i_{qs} + \omega_s\psi_{ds}i_{ds})\} \tag{36}$$

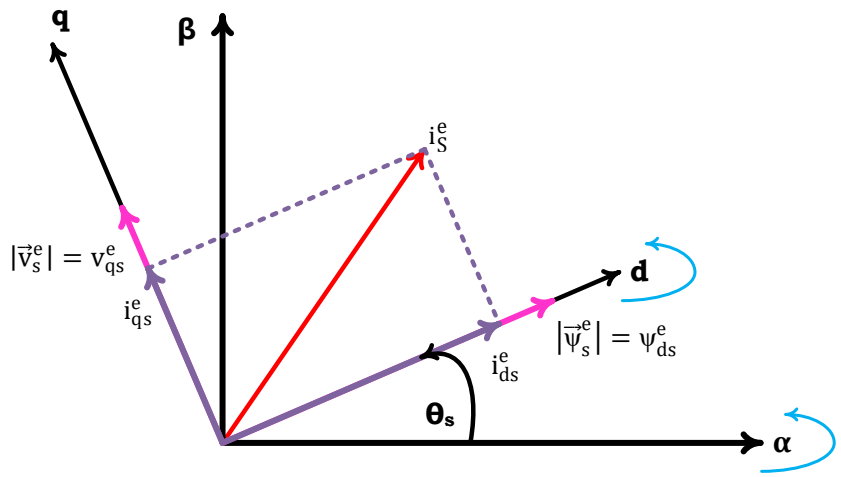

Figure 11. The relation between the flux and stator voltage space vectors [53].

Stator input active and reactive powers can be expressed in terms of the stator flux by separation of Equation (36) into its real and imaginary components, given in Equation (37) and Equation (38) [21, 32]:

$$P_s = \frac{3}{2}\omega_s(\psi_{ds}i_{qs} - \psi_{qs}i_{ds}) \tag{37}$$

$$Q_s = \frac{3}{2}\omega_s(\psi_{ds}i_{ds} + \psi_{qs}i_{qs}) \tag{38}$$

Equation (37) and (38) are derived assuming balanced grid voltage conditions. Under these conditions, the stator flux space vector in the positive synchronous reference frame will be a DC value, therefore it acts as a constant coefficient in the derivation as given in Equation (32).

As demonstrated in the preceding equations, active and reactive powers are less noisy and the output current is less distorted as a result of the reduced distortion in the stator flux compared to the case of voltage-based DPC implementation. This makes it possible to use a lower sampling frequency than what is used in DPC.

However, the required sampling frequency is still much higher than what is needed for FOC and SVM-DPC [54-57]. Equation (30) can be thought of as a first-order filtering of the stator voltage, yielding the stator flux linkage. Therefore, the unbalanced voltage effect on the stator flux is reduced [35].

The proposed stator flux-based DPC approach offers numerous advantages compared to conventional DPC. Several advantages include reduced noise in the output power, decreased current distortion, and lower sampling frequency. However, when compared to FOC, the proposed method suffers from variable switching frequency. Figure 12 depicts the block diagram for the stator flux-based DPC approach.

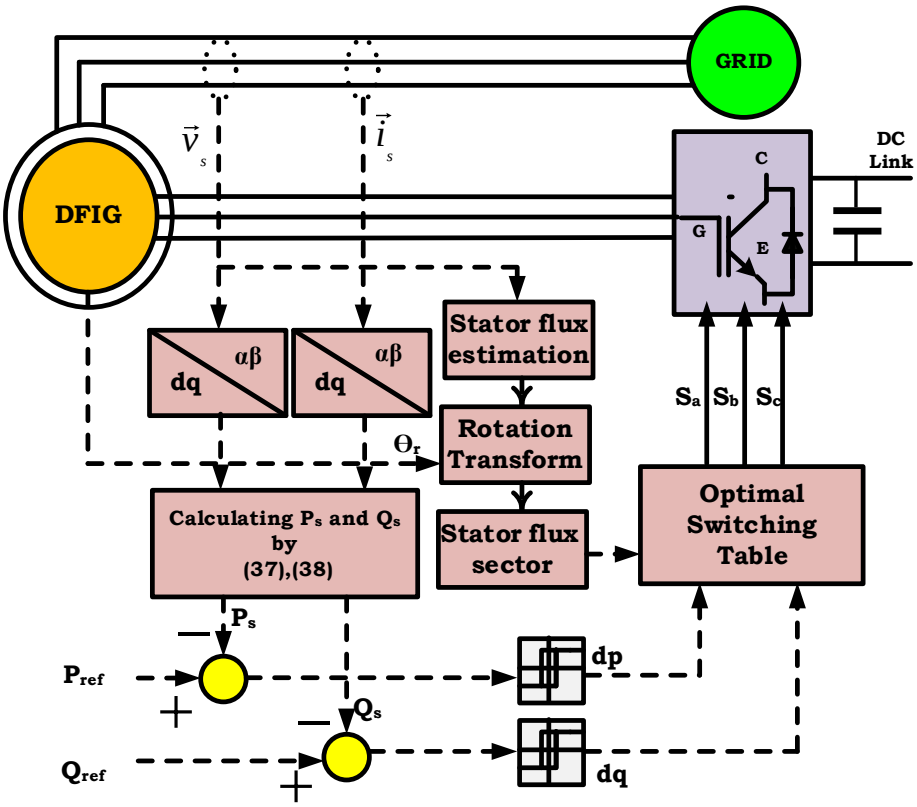

Figure 12. Block diagram of the proposed stator flux-based DPC method.

6. Computer simulation

This section will examine the performance of a grid-connected DFIG system using three controllers: the conventional DPC technique, as well as two DPC methods described in the article. The performance of the DFIG will be examined under both balanced and unbalanced grid voltages. The simulation is performed based on direct power control for the rotor side converter. For this purpose, MATLAB/ Simulink® software is used. The control of the grid-side converter is not addressed in this study. The DFIG parameters are presented in Table 4.

6.1. Direct power control under balanced conditions

In this case, the network voltage is considered balanced. For simplicity, a DC voltage source is used as the DC link in the simulations; in other words, the effect of the grid-side converter is neglected in this study. Figure 13 illustrates the tracking of stator active and reactive powers for a simulation time of four seconds. In the simulation, the stator active and reactive powers are set to -1200 KW and 0 KVAR, respectively. After two seconds, an active power step is applied with a value of 800 KW. Figure 13 demonstrates that the active and reactive powers reach their steady-state values within approximately 0.3 seconds. The rotor speed is taken to be constant throughout the simulation. This controller results in active and reactive powers that track their reference values with some fluctuations; nevertheless, the fluctuations are less than those caused by implementing a direct torque controller. The advantages of this controller include fast dynamic response and a simpler structure than other control algorithms. The following section will evaluate control performance under unbalanced voltage conditions.

Table 4. Simulation Parameters.

Line-to-line RMS voltage	300 V	**Magnetizing inductance**	84.7e-3 H
Stator resistance	0.531 Ω	**Grid frequency (Hz)**	60 Hz
Rotor resistance	0.408 Ω	**Moment of inertia**	0.02 Kg.m^2
Stator leakage inductance	2.5e-3 H	**Frictional coefficient**	0.01 $N.m.\text{sec}/rad$
Rotor leakage inductance	2.5e-3 H	**DC link voltage**	100 V

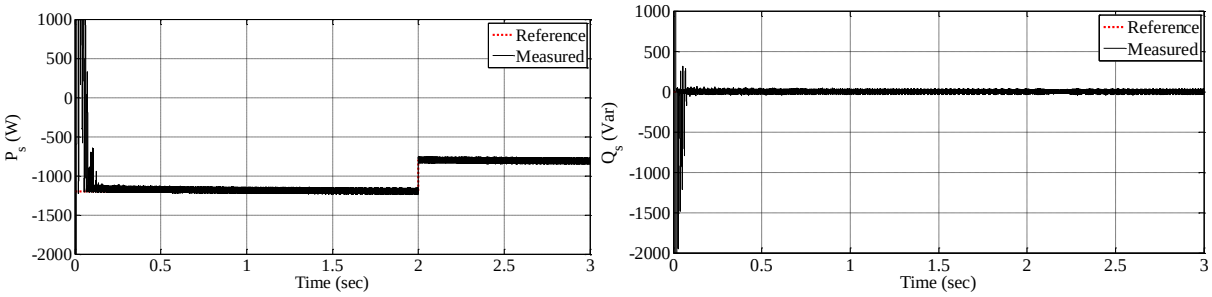

(a) (b)

Figure 13. measured and reference stator a) active power b) reactive power by conventional DPC controller (balanced conditions).

6.2. Direct power control under unbalanced conditions

This section investigates the performance of DFIGs using DPC controllers under unbalanced voltage conditions. Voltage unbalance can occur in the amplitude or phase angle of voltages. In this section, we will run simulations for both unbalances occurring simultaneously. Thus, as illustrated in Figure 14 unbalanced conditions occur within seconds 1-1.5 of simulation. Figures 14(a) and 14(b) show the three-phase stator voltage and current variations, respectively. It has been observed that unbalanced voltages cause harmonic components in stator current. Figure 14(c) depicts the rotor current of one phase. After one second of simulation, it is clear that unbalanced voltages caused deformation and harmonic components in the rotor current.

Figure 15(a) depicts the stator active power under unbalanced conditions, while Figure 15(b) depicts the stator reactive power under unbalanced conditions using conventional direct power control. Figure 15(a) and 15(b) show that a voltage dip (at second 1) caused severe active and reactive power oscillations, which could affect the rotor side converter, given that the converter's rated power is 25-30% of the generator power. After recovering from the voltage dip (at second 1.5), the controller achieves satisfactory performance in terms of tracking the reference powers. Figure 16 illustrates the performance of the proposed DPC method with a PI regulator. As previously stated, the stator current contains some harmonic content when the voltage is unbalanced. In this method, the stator current is first transformed into a positive-synchronous reference frame with the angle determined by the PLL. The proposed (HSF) filter separates the main component from the harmonic components. Only the positive sequence component of the stator current will be passed to the controller, resulting in less active and reactive power oscillations in Figure 16(a) and 16(b).

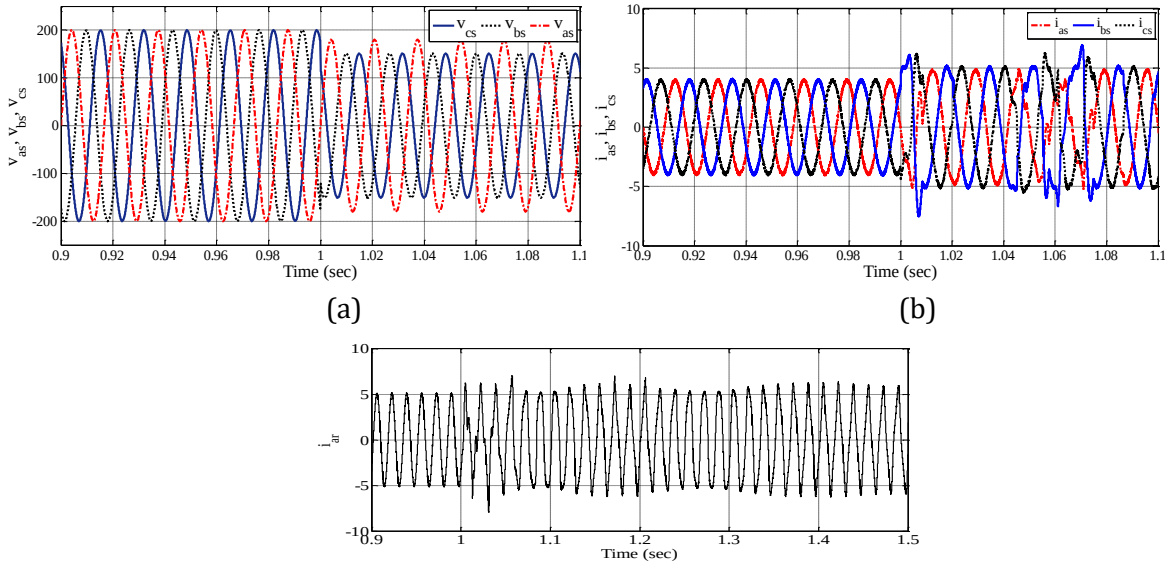

(a) (b)

(c)

Figure 14. a) v_{abcs} b) i_{abcs} c) i_{ar} : before and after voltage unbalance.

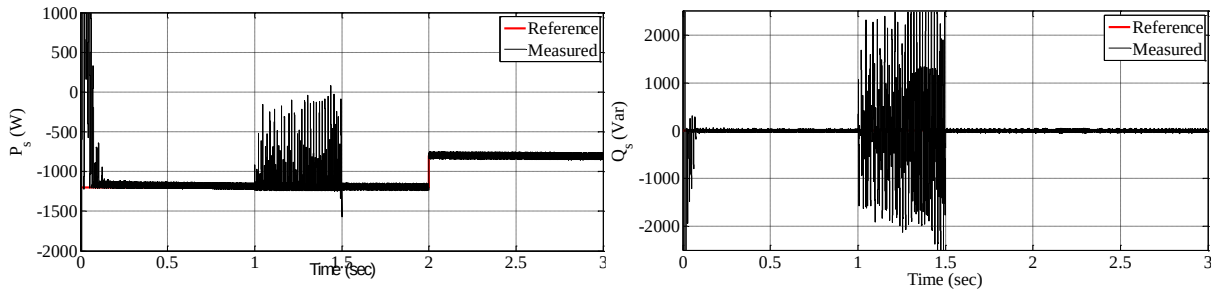

(a) (b)

Figure 15. Measured and reference stator a) active power b) reactive power using conventional DPC controller (unbalanced conditions).

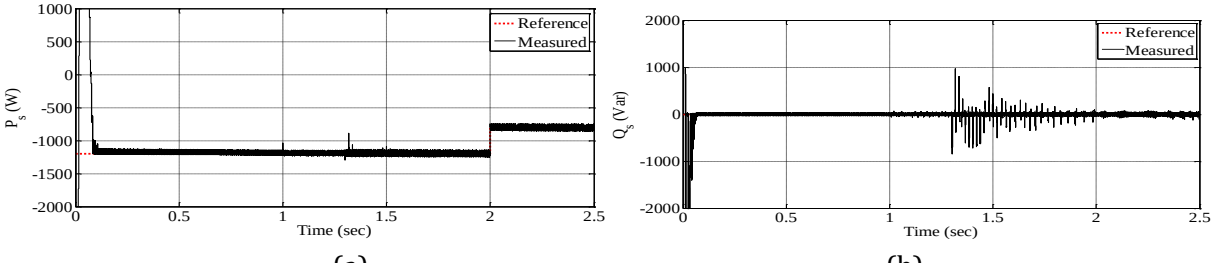

(a) (b)

Figure 16. Measured and reference stator a) active power b) reactive power using the proposed DPC method with PI regulator (unbalanced conditions).

The main advantages of this method are 1) accurate control with less stator harmonic current than conventional DPC, and 2) reduced stator power ripple. The main disadvantages of this method are increased implementation costs and a reduction in simulation speed due to the use of PI controllers. Figure 17 shows the positive, negative, and zero sequence components of the stator current. It is observed that the proposed control approach has resulted in stator currents with negligible negative and zero sequence components.

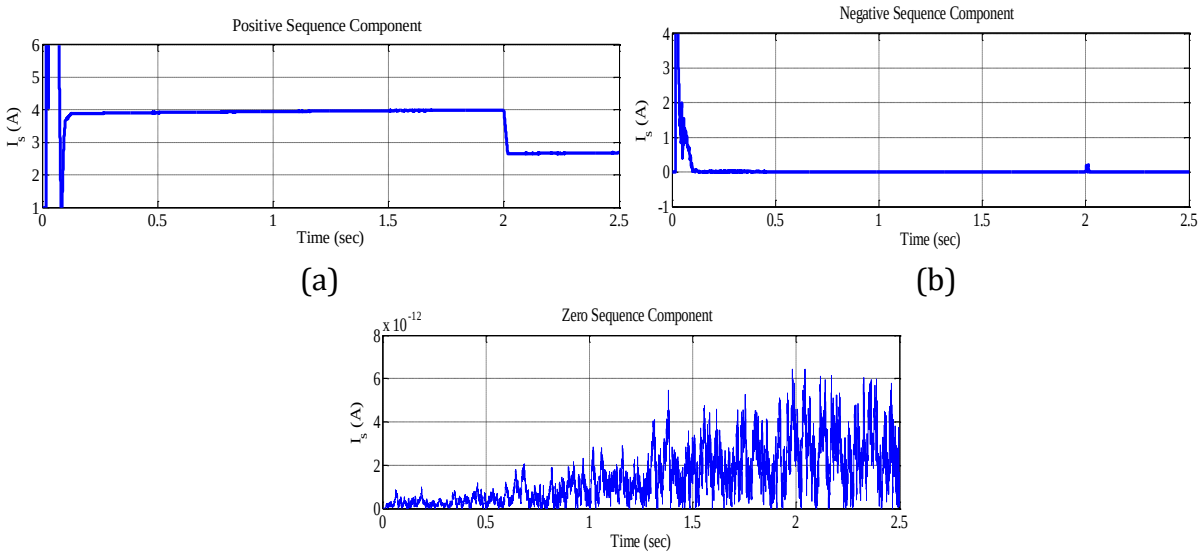

Figure 17. a) positive sequence, b) negative sequence, and c) zero sequence components of stator current.

Figure 18 depicts the stator and rotor currents for the proposed DPC method with a PI regulator under unbalanced voltage conditions. This method significantly reduces stator current distortion and produces sinusoidal currents. Figure 18(b) shows less rotor current deformation after 1 second compared to Figure 14(c), indicating superior control performance. Figure 19(a) and 19(b) illustrate the measured stator active and reactive powers using the proposed stator flux-based DPC method. As shown in the figures, the proposed control performs better with less oscillation than the conventional DPC.

The active and reactive power ripples have been significantly reduced, eliminating the need for positive and negative sequence separation. This controller can be used to stabilize the DC link voltage and regulate power exchange with the network and converter. The simulation results also show that the stator current has a lower THD. Unbalanced voltage has a smaller effect on stator flux than stator voltage, so power ripple is reduced. Figure 20 depicts a three-phase stator current and single-phase rotor current under unbalanced voltage conditions.

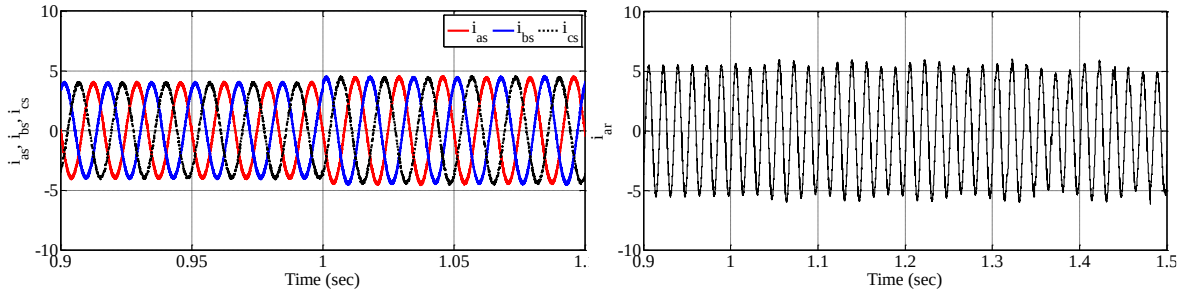

Figure 18. DFIG a) stator current b) rotor current using the proposed DPC with PI regulator under unbalanced conditions.

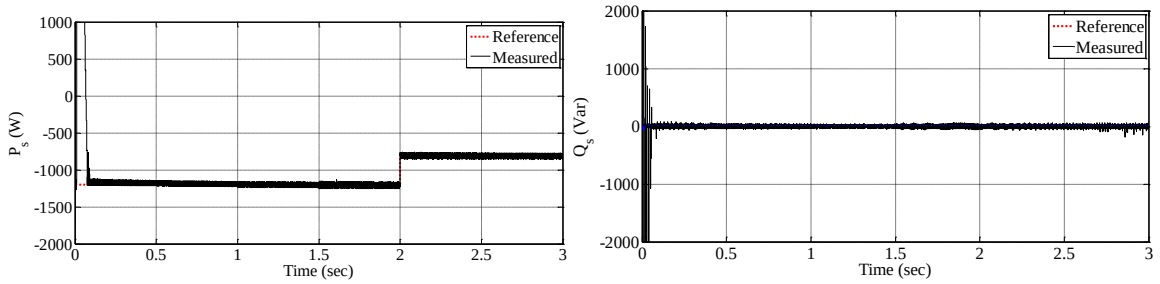

(a) (b)

Figure 19. Measured and reference stator a) active power b) reactive power using the proposed stator flux-based DPC controller under unbalanced conditions.

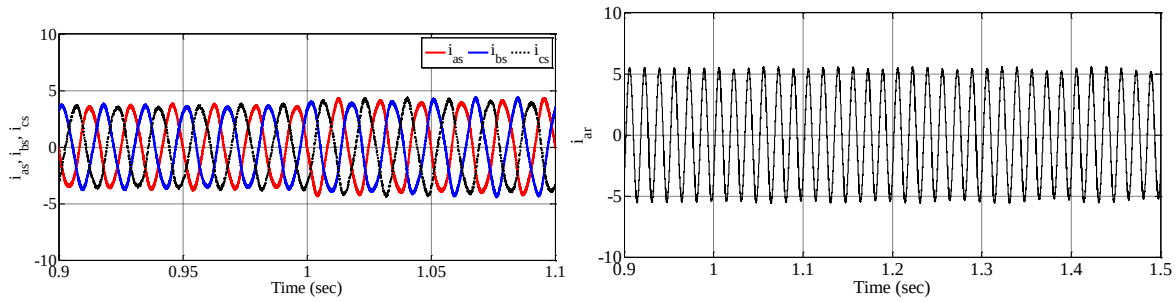

(a) (b)

Figure 20. DFIG a) stator current b) rotor current using the proposed stator flux-based DPC controller under unbalanced conditions**.**

The proposed method leads to less distortion of stator and rotor currents in comparison to Figure 14. Figure 21(a) and 21(b) show the stator current THD under unbalanced conditions for the conventional DPC method and the proposed DPC method with PI regulator, respectively. As shown in the figure, the stator current THD with the proposed DPC method with PI regulator is significantly lower than with the conventional DPC method. The main harmonics in DPC with PI regulator are the third, fifth, and seventh.

The main harmonics for the stator flux-based DPC method are the third and fifth harmonics, as Figure 21(c) illustrates. This figure shows that THD is significantly lower than with the conventional DPC method under unbalanced grid voltage conditions. While the conventional DPC method experiences power and torque fluctuations under unbalanced voltage conditions, the proposed methods provide a smoother, less fluctuating, and faster dynamic response in the event of voltage unbalanced or dip conditions.

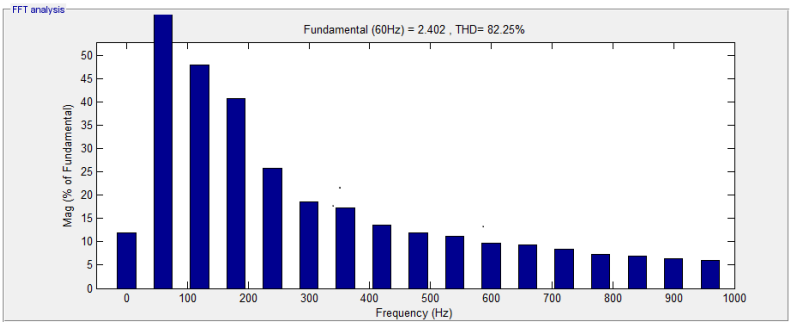

(a)

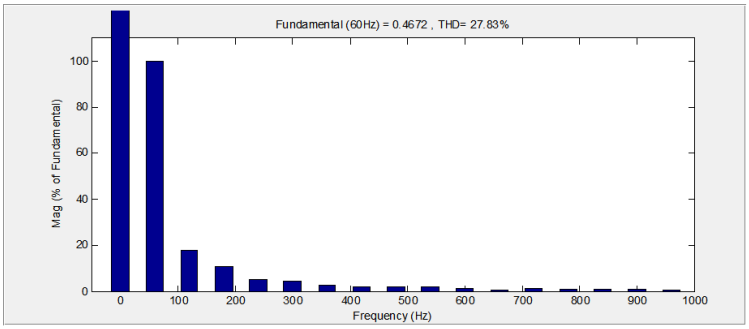

(b)

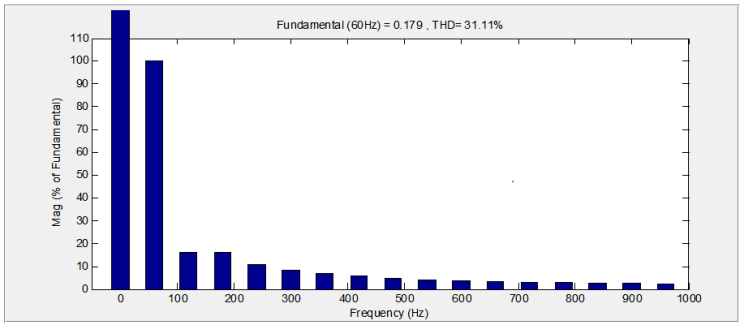

(c)

Figure 21. stator current THD under unbalanced conditions, a) Conventional DPC method, b) Proposed DPC method with PI regulator, c) Proposed stator flux-based DPC method**.**

In this paper, in the first proposed method, a novel HSF filter was proposed to extract the fundamental component of stator current and inject it into the controller during fault conditions; it was observed that the proposed controller can mitigate power and torque fluctuations while also reducing stator current THD. Using hysteresis comparators resulted in faster dynamic response and greater robustness than PWM techniques. The flux-based stator DPC method was the second alternative to the conventional DPC method. The simulation results demonstrate the efficacy of this method. Table 5 is provided for a comprehensive comparison of the approaches. The table differentiates between the structure and performance of the proposed PI-DPC method and the stator flux-based DPC method compared to the conventional DPC method.

Table 5. comparison of the proposed PI-DPC method and Stator flux-based DPC method with the conventional DPC method**.**

	PI-DPC	Stator flux-based DPC
Generator power ripple	Lower	Lower
Rotor speed ripple	Lower	Lower
RSC PWM	No	No
Number of PI controllers	Two	-
Controller bandwidth	Higher	Higher
Steady-state response	Smoother	Smoother
Transient response	slower with less overshoot and fluctuations	Faster with less overshoot and fluctuations
Complexity	More	Similar
Current THD	Lower	Lower

7. Conclusion

This paper described theoretical improvements in DFIG-based wind energy conversion systems under balanced and unbalanced grid voltage conditions. A dynamic model based on space vector relations in the rotor reference frame was examined. In the next step, the performance of DFIG under unbalanced voltage conditions was investigated. It was demonstrated that unbalanced voltages result in both positive and negative components in the current and voltage, which contribute to an increase in active and reactive power ripple as well as current THD. Methods for improving DFIG performance were briefly introduced. Direct power control with a PI regulator results in better performance and less power ripple due to the injection of positive sequence components of stator current into the controller under unbalanced voltage conditions. Stator flux-based DPC combines the advantages of DPC and FOC. These benefits include a low THD of the output currents and a straightforward implementation process (in comparison to predictive DPC). Additionally, this controller is more cost-effective than other options that were examined, and it also produces lower power ripples. Simulation results confirmed an improvement in control system performance compared to conventional DPC without requiring significant changes to the controller structure. The THD of stator current under unbalanced conditions was found to be approximately 82% for the conventional DPC method, while it was reduced to approximately 27% and 31% for the proposed DPC methods with PI regulator and stator flux-based method, respectively. The direct power control method is compared to other control methods, including predictive control, vector control, direct torque control, and DPC-SVM. Although it improves control and reduces oscillations in power and switching frequency, it also increases controller complexity and slows dynamic response. To enhance the reactive power capability and voltage stability of the wind turbine system, it is recommended to integrate a static compensator (STATCOM) at the connection point in future work.

APPENDIX A:

The moduli of stator flux ($\left|\vec{\psi}_s^r\right|$) are constant due to direct connection to the grid. The following expressions are used:

$$\vec{i}_s^r = \frac{\vec{\psi}_s^r}{\sigma L_s} - \frac{\vec{\psi}_r^r L_m}{\sigma L_s L_r} \qquad \text{(a1)}$$

$$\dot{\vec{\psi}}_s^r = \left|\vec{\psi}_s^r\right| j\dot{\theta}_s e^{j\omega_s t} = j(\omega_s - \omega_m)\vec{\psi}_s^r$$

Replacing $\vec{i}_s^r$ and $\dot{\vec{\psi}}_s^r$ in (1) gives:

$$P_s = \frac{3}{2}\mathrm{Re}\{(j(\omega_s - \omega_m)\vec{\psi}_s^r + j\omega_m\vec{\psi}_s^r)\cdot(\frac{\vec{\psi}_s^r}{\sigma L_s} - \frac{L_m\vec{\psi}_r^r}{\sigma L_s L_r})^*\} = \frac{3}{2}\mathrm{Re}\{(j(\omega_s\vec{\psi}_s^r)\cdot(\frac{\vec{\psi}_s^r}{\sigma L_s} - \frac{L_m\vec{\psi}_r^r}{\sigma L_s L_r})^*\}$$

Keeping in mind that:

$$\frac{3}{2}\mathrm{Re}\{(j(\omega_s\vec{\psi}_s^r)\cdot(\frac{\vec{\psi}_s^r}{\sigma L_s})^*\} = 0$$

The active power expression can be simplified as follows:

$$P_s = -\frac{3}{2}\frac{L_m}{\sigma L_s L_r}\omega_s \operatorname{Re}\{(j\vec{\psi}_s^r \vec{\psi}_r^{r*})\} \quad \text{(a2)}$$

This can also be written in terms of the moduli of stator flux, moduli of rotor flux, and the angle (θ_ψ) between them:

$$P_s = -\frac{3}{2}\frac{L_m}{\sigma L_s L_r}\omega_s \left|\vec{\psi}_s^r\right|\left|\vec{\psi}_r^r\right|\cos(90-\theta_\psi)$$
$$P_s = -\frac{3}{2}\frac{L_m}{\sigma L_s L_r}\omega_s \left|\vec{\psi}_s^r\right|\left|\vec{\psi}_r^r\right|\sin\theta_\psi \quad \text{(a3)}$$

Similarly, replacing (a1) in (2) gives:

$$Q_s = -\frac{3}{2}\operatorname{Im}\{(j(\omega_s-\omega_m)\vec{\psi}_s^r + j\omega_m\vec{\psi}_s^r).(\frac{\vec{\psi}_s^r}{\sigma L_s} - \frac{L_m\vec{\psi}_r^r}{\sigma L_s L_r})^*\} = -\frac{3}{2}\operatorname{Im}\{(j(\omega_s\vec{\psi}_s^r).(\frac{\vec{\psi}_s^r}{\sigma L_s} - \frac{L_m\vec{\psi}_r^r}{\sigma L_s L_r})^*\}$$

$$= -\frac{3}{2}\frac{\omega_s}{\sigma L_s}\operatorname{Im}\{j\vec{\psi}_s^r.\vec{\psi}_s^{r*} - j\vec{\psi}_s^r\frac{L_m}{L_r}\vec{\psi}_r^{r*}\} = -\frac{3}{2}\frac{\omega_s}{\sigma L_s}.\left|\vec{\psi}_s^r\right|^2 + \frac{3}{2}\frac{\omega_s}{\sigma L_s}\frac{L_m}{L_r}\operatorname{Im}\{j\vec{\psi}_s^r\vec{\psi}_r^{r*}\}$$

Using the identity

$$\operatorname{Im}\{j\vec{\psi}_s^r\vec{\psi}_r^{r*}\} = \operatorname{Re}\{\vec{\psi}_s^r\vec{\psi}_r^{r*}\}$$

Stator reactive power can be written as (a4):

$$Q_s = \frac{3}{2}\frac{\omega_s}{\sigma L_s}\left|\vec{\psi}_s^r\right|(\frac{L_m}{L_r}\left|\vec{\psi}_r^r\right|\cos\theta_\psi - \left|\vec{\psi}_s^r\right|) \quad \text{(a4)}$$

References

[1] S. E. Aimani, "Modeling and Control Structures for Variable Speed Wind Turbine." *International Conference on Multimedia Computing and Systems*, pp. 1-5, 2011.

[2] F. Iov, and F. Blaabjerg, "Power Electronics and Control for Wind Power Systems." *Power Electronics and Machines in Wind Applications proceedings of international conference in Lincoln, USA*, pp. 1-16. 2009.

[3] R. Cardenas, R. Peña, S. Alepuz, and G. Asher, "Overview of Control Systems for the Operation of DFIGs in Wind Energy Applications," *IEEE Transactions on Industrial Electronics*, vol. 60, no. 7, pp. 2776-2798, 2013.

[4] A. Bouafia, F. Krim, and J. P. Gaubert, "Design and Implementation of High Performance Direct Power Control of Three-Phase PWM Rectifier, via Fuzzy and PI Controller for Output Voltage Regulation," *Energy conversion and management*, vol. 50, no. 1, pp. 6-13, 2009.

[5] J. Hu, L. Shang, Y. He, and Z. Q. Zhu, "Direct Active and Reactive Power Regulation of Grid-Connected DC/AC Converters Using Sliding Mode Control Approach," *IEEE transactions on power electronics*, vol. 26, no. 1, pp. 210-222, 2010.

[6] P. Antoniewicz, and M. P. Kazmierkowski, "Virtual-Flux-Based Predictive Direct Power Control of AC/DC Converters with Online Inductance Estimation," *IEEE Transactions on Industrial Electronics*, vol. 55, no. 12, pp.4381-4390, 2008.

[7] S. Peresada, A. Tilli, and A. Tonielli, "Indirect Stator Flux-Oriented Output Feedback Control of a Doubly Fed Induction Machine," *IEEE Transactions on Control Systems Technology*, vol. 11, no. 6 pp. 875-888, 2003.

[8] A. Ramkumar, S. Durairaj, and K. Dhivya, "Behavior of DFIG With Direct Torque Controller at Unbalanced and Distorted Grid Voltage Conditions," *Applied Mechanics and Materials*, vol. 626, pp. 150-154, 2014.

[9] S. Arnalte, J. C. Burgos, and J. L. Rodriguez-Amenedo, "Direct Torque Control of A Doubly-Fed Induction Generator for Variable Speed Wind Turbines," *Electric power components and systems*, vol. 30, no. 2, pp. 199-216, 2002.
[10] Y. Djeriri, A. Meroufel, A. Massoum, and Z. Boudjema, "A Comparative Study Between Field Oriented Controlstrategy and Direct Power Control Strategy for DFIG," *Journal of Electric Engineering*, vol. 14, no. 2, pp. 9-9, 2014.
[11] M. Malinowski, M. Jasinski, and M. P. Kazmierkowski, "Simple Direct Power Control of Three-Phase PWM Rectifier using Space-Vector Modulation (DPC-SVM)," *IEEE Transactions on Industrial Electronics*, vol. 51, no. 2, pp. 447-454, 2004.
[12] S. A. Larrinaga, M. A. Rodriguez Vidal, E. Oyarbide, and J. R. Torrealday Apraiz, "Predictive Control Strategy for DC/AC Converters Based on Direct Power Control," *IEEE Transactions on Industrial Electronics*, vol. 54, no. 3, pp. 1261-1271, 2007.
[13] W. S. Kim, S. T. Jou, K. B. Lee, and S. Watkins, "Direct Power Control of a Doubly Fed Induction Generator with a Fixed Switching Frequency," *IEEE Industry Applications Society Annual Meeting*, pp. 1-9, 2008.
[14] D. Casadei, G. Serra, and A. Tani, "Improvement of Direct Torque Control Performance by using a Discrete SVM Technique," *29th Annual IEEE Power Electronics Specialists Conference (Cat. No. 98CH36196)*, vol. 2, pp. 997-1003, 1998.
[15] D. Sun, and X. Wang, "Low-Complexity Model Predictive Direct Power Control for DFIG Under Both Balanced and Unbalanced Grid Conditions," *IEEE Transactions on Industrial Electronics*, vol. 63, no. 8, pp. 5186-5196, 2016.
[16] Y. Zhang, J. Jiao, et al., "Model Predictive Direct Power Control of Doubly Fed Induction Generators Under Balanced and Unbalanced Network Conditions," *IEEE Transactions on Industry Applications*, vol. 56, no. 1, pp. 771-786, 2019.
[17] M. E. Zarei, C. Veganzones Nicolás, and J. Rodríguez Arribas, "Improved Predictive Direct Power Control of Doubly Fed Induction Generator During Unbalanced Grid Voltage Based on Four Vectors," *IEEE Journal of Emerging and Selected Topics in Power Electronics*, vol. 5, no. 2, pp. 695-707, 2016.
[18] L. Li, H. Nian, L. Ding, and B. Zhou, "Direct Power Control of DFIG System Without Phase-Locked Loop Under Unbalanced and Harmonically Distorted Voltage," *IEEE Transactions on Energy Conversion*, vol. 33, no. 1, pp. 395-405, 2017.
[19] E. Ozsoy, B. Soner, et al., "Disturbance Observer Based Power Control of DFIG Under Unbalanced Network Conditions," *Electric Power Components and Systems*, vol. 46, no. 13, pp. 1448-1461, 2018.
[20] M. Jahanpour-Dehkordi, S. Vaez-Zadeh, and J. Mohammadi, "Development of a Combined Control System to Improve the Performance of a PMSG-Based Wind Energy Conversion System Under Normal and Grid Fault Conditions," *IEEE Transactions on Energy Conversion*, vol. 34, no. 3, pp. 1287-1295, 2019.
[21] S. S. Lee, and Y. E. Heng, "Table-Based DPC for Grid Connected VSC under Unbalanced and Distorted Grid Voltages: Review and Optimal Method," *Renewable and Sustainable Energy Reviews*, vol. 76, pp. 51-61, 2017.
[22] A. Izanlo, S. A. Gholamian, and M. V. Kazemi, "Using of Four-Switch Three-Phase Converter in the Structure DPC of DFIG Under Unbalanced Grid Voltage Condition," *Electrical Engineering*, vol. 100, no. 3, pp. 1925-1938, 2018.
[23] J. Mohammadi, S. Vaez-Zadeh, S. Afsharnia, and E. Daryabeigi, "A Combined Vector and Direct Power Control for DFIG-Based Wind Turbines," *IEEE Transactions on Sustainable Energy*, vol. 5, no. 3, pp. 767-775, 2014.
[24] G. N. González, C. H. De Angelo, and D. A. Aligia, "A Control Strategy for DFIG-Based Systems Operating under Unbalanced Grid Voltage Conditions," *International Journal of Electrical Power & Energy Systems*, vol. 142, 108273, 2022.
[25] P. Cheng, C. Wu, F. Ning, and J. He, "Voltage Modulated DPC Strategy of DFIG Using Extended Power Theory under Unbalanced Grid Voltage Conditions," *Energies*, vol. 13, no. 22, p. 6077, 2020.
[26] E. G. Shehata, "Improved Power Control of DFIGs Driven by Wind Turbine under Unbalanced Grid Voltage," *Journal of Electrical Engineering & Technology*, vol. 19, no. 1, pp. 325-340, 2024.

[27] S. Gao, H. Zhao, et al., "Novel Direct Power Control for DFIG With Parallel Compensator under Unbalanced Grid Condition," *IEEE Transactions on Industrial Electronics*, vol. 68, no. 10, pp. 9607-9618, 2021.

[28] S. Das, and B. Singh, "Enhanced Control of DFIG Based Wind Energy Conversion System Under Unbalanced Grid Voltages Using Mixed Generalized Integrator," *IEEE Journal of Emerging and Selected Topics in Industrial Electronics*, vol. 3, no. 2, pp. 308-320, 2020.

[29] X. Ran, B. Xu, K. Liu, and J. Zhang, " An Improved Low-Complexity Model Predictive Direct Power Control with Reduced Power Ripples Under Unbalanced Grid Conditions" *IEEE Transactions on Power Electronics*, vol. 37, no. 5, pp. 5224-5234, 2022.

[30] L. Xu, and Y. Wang, "Dynamic Modeling and Control of DFIG-Based Wind Turbines Under Unbalanced Network Conditions," *IEEE Transactions on Power Systems*, vol. 22, no. 1, pp. 314-323, 2007.

[31] L. Xu, and P. Cartwright, "Direct Active and Reactive Power Control of DFIG for Wind Energy Generation," *IEEE Transactions on energy conversion*, vol 21, no. 3, pp. 750-758, 2006.

[32] G. Abad, J. Lopez, M. Rodriguez, L. Marroyo, and G. Iwanski, "Doubly fed induction machine: modeling and control for wind energy generation," vol. 85. *John Wiley & Sons*, 2011.

[33] Y. Zhang, C. Qu, Z. Li, and Y. Zhang, "Mechanism Analysis and Experimental Study of Table-Based Direct Power Control," *International Conference on Electrical Machines and Systems (ICEMS)*, pp. 2213-2218, 2013.

[34] F. Senani, A. Rahab, F. Louar, F. Bourourou, and H. Benalla, "Active and Reactive Power Control of DFIG using PI and DPC Controllers," *International Conference on Electrical Engineering (ICEE)*, pp. 1-6, 2015.

[35] M. Malinowski, M. P. Kazmierkowski, S. Hansen, F. Blaabjerg, and G. Marques. "Virtual Flux Based Direct Power Control of Three-Phase PWM Rectifiers," *IEEE Transactions on Industry Applications*, vol. 37, no. 4, pp. 1019-1027, 2001.

[36] J. Hu, J. Zhu, et al., "Predictive Direct Virtual Torque and Power Control of Doubly Fed Induction Generators for Fast and Smooth Grid Synchronization and Flexible Power Regulation," *IEEE Transactions on Power Electronics*, vol. 28, no. 7, pp. 3182-3194, 2012.

[37] G. Abad, M. Á. Rodríguez, and J. Poza, "Two-Level VSC Based Predictive Direct Torque Control of the Doubly Fed Induction Machine with Reduced Torque and Flux Ripples at Low Constant Switching Frequency," *IEEE transactions on power electronics*, vol. 23, no. 3, pp. 1050-1061, 2008.

[38] W. Wenjun, Z. Yanru, and W. Jianjun, "The Comparative Study of Different Methods About Constructing Switching Table in DPC for Three-Level Rectifier," *The 2nd International Symposium on Power Electronics for Distributed Generation Systems*, pp. 314-319, 2010.

[39] A. Hemdani, M. J. B. Ghorbal, M. W. Naouar, and I. Slama-Belkhodja, "Design of A Switching Table for Direct Power Control of a DFIG using Sliding Mode Theory," *Eighth International Multi-Conference on Systems, Signals & Devices*, pp. 1-7, 2011.

[40] J. Eloy-Garcia, and R. Alves, "DSP-Based Direct Power Control of a VSC with Voltage Angle Estimation," *IEEE/PES Transmission & Distribution Conference and Exposition: Latin America*, pp. 1-5, 2006.

[41] K. Kulikowski, and A. Sikorski, "New DPC Look-Up Table Methods for Three-Level AC/DC Converter," *IEEE Transactions on Industrial Electronics*, vol. 63, no. 12, pp. 7930-7938, 2016.

[42] Y. Zhang, and C. Qu, "Table-Based Direct Power Control for Three-Phase AC/DC Converters Under Unbalanced Grid Voltages," *IEEE Transactions on Power Electronics*, vol. 30, no. 12, pp. 7090-7099, 2015.

[43] A. Ben Amer, S. Belkacem, and T. Mahni, "Direct Torque Control of a Doubly Fed Induction Generator," *International Journal of Energetica*, vol. 2, no. 1, pp. 11-14, 2017.

[44] T. Noguchi, H. Tomiki, S. Kondo, and I. Takahashi, "Direct Power Control of PWM Converter without Power Source Voltage Sensors," *IAS'96. Conference Record of the 1996 IEEE Industry Applications Conference Thirty-First IAS Annual Meeting*, vol. 2, pp. 941-946, 1996.

[45] M. J. Zandzadeh, and A. Vahedi, "Modeling and Improvement of Direct Power Control of DFIG under Unbalanced Grid Voltage Condition," *International Journal of Electrical Power & Energy Systems*, vol. 59, pp. 58-65, 2014.

[46] T. Brekken, N. Mohan, and T. Undeland, "Control of a Doubly-Fed Induction Wind Generator Under Unbalanced Grid Voltage Conditions," *European Conference on Power Electronics and Applications*, pp. 10, 2005.
[47] F. Soares dos Reis, J. A. V. Alé, et al., "Active Shunt Filter for Harmonic Mitigation in Wind Turbines Generators," *37th IEEE Power Electronics Specialists Conference*, pp. 1-6, 2006.
[48] S. A. Papathanassiou, and M. P. Papadopoulos, "Harmonic Analysis in a Power System with Wind Generation," *IEEE Transactions on power delivery*, vol. 21, no. 4, pp. 2006-2016, 2006.
[49] S. K. Jain, and P. Agarwal, "Design Simulation and Experimental Investigations, on a Shunt Active Power Filter for Harmonics, and Reactive Power Compensation," *Electric Power Components and Systems*, vol. 31, no.7, pp.671-692, 2003.
[50] D. De Santis, and M. Chen, "Design of Active Low Pass Filters to Reduce Harmonic Current Emission," *IECON 2017-43rd Annual Conference of the IEEE Industrial Electronics Society*, pp. 1059-1065, 2017.
[51] A. Gaillard, P. Poure, S. Saadate, and M. Machmoum, "Variable Speed DFIG Wind Energy System for Power Generation and Harmonic Current Mitigation," *Renewable Energy*, vol. 34, no. 6, pp. 1545-1553, 2009.
[52] H. S. Song, H. G. Park, and K. Nam, "An Instantaneous Phase Angle Detection Algorithm under Unbalanced Line Voltage Condition," *Annual IEEE Power Electronics Specialists Conference. Record. (Cat. No.99CH36321),* pp. 533-537, 1999.
[53] F. Mulolani, "Performance of Direct Power Controlled Grid-Connected Voltage Source Converters," Ph.D. dissertation, Newcastle University, 2017.
[54] M. P. Kazmierkowski, R. Krishnan, F. Blaabjerg, and J. D. Irwin, Eds., "Control in Power Electronics: Selected Problems", Academic Press, 2002.
[55] S. Kouadria, E. M. Berkouk, Y. Messlem, and M. Denai, "Improved Control Strategy of DFIG-Based Wind Turbines using Direct Torque and Direct Power Control Techniques," *Journal of Renewable and Sustainable Energy*, vol. 10, no. 4, 2018.
[56] T. Sutikno, N. R. N. Idris, and A. Jidin, "A Review of Direct Torque Control of Induction Motors for Sustainable Reliability snd Energy Efficient Drives," *Renewable and sustainable energy reviews*, vol. 32, pp. 548-558, 2014.
[57] P. Gajewski, and K. Pieńkowski, "Advanced Control of Direct-Driven PMSG Generator in Wind Turbine System," *Archives of Electrical Engineering*, vol. 65, no. 4, pp.643-656, 2016.

Declaration of Competing Interest

The authors declare that they have no known competing financial interests or personal relationships that could have appeared to influence the work reported in this paper. The ethical issues, including plagiarism, informed consent, misconduct, data fabrication and/or falsification, double publication and/or submission, redundancy, have been completely observed by the authors.

Credit Authorship Contribution Statement

Mohammad Naser Hashemnia: Conceptualization, Formal analysis, Investigation, Methodology, Resources, Software, Supervision, Validation, Visualization, Roles/Writing-original draft, Writing-review & editing. **Ali Dehghan Nayeri:** Conceptualization, Software, Validation, Roles/Writing-original draft.

Bibliography

Mohammad Naser Hashemnia was born in Mashhad, Iran, in 1983. He received the B.S. degree in electrical power engineering from Ferdowsi University, Mashhad, Iran, in 2006 and the M.S. degree in electrical power engineering from the University of Tehran, Tehran, Iran, in 2008. He earned his Ph.D. degree in electrical power engineering from Sharif University of Technology, Tehran, Iran in 2013. Since 2015 he has been an assistant professor in Mashhad branch, Islamic Azad University, Mashhad, Iran. His primary research interests are electric machine analysis, modeling, and simulation, innovative electrical drive control approaches, and renewable energy systems.

Ali Dehghan Nayeri was born in Mashhad, Iran, in 1991. He received the B.S. degree in electronic engineering from Eqbal lahoori University, Mashhad, Iran, in 2014 and the M.S. degree in electrical power and renewable energy from Islamic Azad University, Mashhad, Iran, in 2019. His main research interests include analysis, programing and simulation of electric machines, automation and programming control and artificial intelligence.